NUMERICAL SIMULATION OF INCLUSION AGGREGATION AND REMOVAL IN THE GAS-STIRRED LADLE

by

Xipeng Guo

A Thesis

Submitted to the Faculty of Purdue University

In Partial Fulfillment of the Requirements for the degree of

Master of Science in Mechanical Engineering

Department of Mechanical and Civil Engineering

Hammond, Indiana

December 2019

THE PURDUE UNIVERSITY GRADUATE SCHOOL
STATEMENT OF COMMITTEE APPROVAL

Dr. Chenn Q. Zhou, Chair
Department of Mechanical and Civil Engineering

Dr. Xiuling Wang
Department of Mechanical and Civil Engineering

Dr. Ran Zhou
Department of Mechanical and Civil Engineering

Approved by:
Dr. Chenn Q. Zhou

To the people I love

ACKNOWLEDGMENTS

I would like to express my deepest appreciation to all those who provided me the possibility to complete this thesis. A greatest gratitude I give to my advisor, Prof. Chenn Q Zhou. It is she who offered the opportunity for me to study at Purdue. With her careful guidance and encouragement, I can successfully complete the thesis. I would like to thank Prof. Xiuling Wang and Prof. Ran Zhou for serving on my advisory committee and providing valuable suggestions and comments during the course and thesis of study.

I would like to thank the colleagues in the Center for Innovation through Visualization and Simulation (CIVS) at Purdue University Northwest for their kind help and encourage to me. A special gratitude I would like to give to my CIVS mentor, Dr. Armin Silaen, whose professional advice help me a lot during the study of the thesis. Without his help, I will spend much more time exploring right direction.

I would like to acknowledge support from the Steel Manufacturing Simulation and Visualization Consortium (SMSVC) throughout the course of this research.

I would like to thank my parents, the people who love me and the people that I love. Thank them for giving me the strength and encouragement to complete my studies.

TABLE OF CONTENTS

LIST OF TABLES

LIST OF FIGURES

LIST OF SYMBOLS

A	Inclusion aggregation rate (m^3/s)
A_e	Slag eye area (m^2)
A_{isb}	Hamaker constant for inclusion - bubble collision, 6.47×10^{19} J
A_{isi}	Hamaker constant for inclusion - inclusion collision, 3.98×10^{19} J
A_s	Local slag cell effective area (m^2)
C	Constant
d	Diameter (m)
E_{csu}	Collision efficiency
E_0	Eotvos number
E_{Shear}	Inclusion-inclusion shear collision efficiency
E_{Stokes}	Collision efficiency
F_b	Force from bubble (N)
F_D	Drag force (N)
$F_{pressure}$	Pressure gradient force (N)
F_{VM}	Virtual mass force (N)
G_b	Turbulence kinetic energy generation due to buoyangcy (m^2/s^2)
G_k	Turbulence kinetic energy generation due to velocity gradient (m^2/s^2)
g	Gravity acceleration (m/s^2)
H	Ladle height (m)
h	Slag thickness (m)
K	Kolmogorov microscale (m)
k	Turbulence kinetic energy (m^2/s^2)
N_s	Stokes number
$n(V_j, t)$	number density of j size inclusions ($n/m^3 s$)
p	Pressure (Pa)
Q	Argon gas flow rate (m^3/s)
R	Inclusion removal rate ($n/m^3 s$)

Re	Reynolds Number
r	Inclusion radius (m)
S	Source term ($kg/m^3 s$)
u_p^S	Stokes velocity of rising particles (m/s)
u_j^T	Turbulence velocity to size j inclusion (m/s)
u	Velocity (m/s)
V_{cell}	Local slag cell volume (m^3)
α	Volume fraction of inclusion phase at t seconds
γ	Inclusion removal rate
θ	Particle colliding angle
ρ	Density (kg/m^3)
σ	Surface tension (N/m)
ε	Turbulence dissipation rate (m^2/s^3)
μ	Dynamic viscosity, ($Pa.s$)
ϑ	Kinetic viscosity (m^2/s)
$\bar{\bar{\tau}}$	Stress-strain tensor (Pa)
τ_{rel}	Relaxation time of bubble (s)
τ_B	Bubble breakup timescale (s)
τ_C	Bubble coalescence timescale (s)
τ_b	Time scale of bubble relaxation (s)
τ_l	Time scale of energetic turbulence eddies (s)

SUBSCRIPT

i	Inclusion phase
j, k	Inclusion group size
l	Liquid steel
m, n	Continuum phase index
p	Tracked particle
s	slag
t	Time

SUPERSCRIPT

i-b	Inclusion collide with bubble
i-i	Inclusion collide with inclusion
BF	Inclusion removal due to buoyancy collision
slag	Inclusion removal due to slag absorption
TS	Turbulence shear collision
TR	Turbulence random collision
wall	Inclusion removal due to wall adhesion
wake	Inclusion removal due to bubble wake

ABSTRACT

A comprehensive study of inclusion aggregation and removal in different bottom gas-stirred ladles has been conducted. The unsteady, three dimensional, isothermal, multiphase computational fluid dynamics (CFD) model was developed. A ladle with two bottom plugs was used in the study. Effects of plug separation angles (180° and 90°) and argon flow rate combinations (5/5 SCFM, 5/20 SCFM and 20/20 SCFM) were investigated. The whole study can be divided into two parts: first, the flow field, slag eye size and wall shear stress have been studied; second, inclusion aggregation and removal in different ladles have been investigated.

In the first part, argon bubble breakup and coalescence has been considered. The slag eye size was validated with plant measurement. When the flow rate increases, the size of slag eye will increase while the wall shear stress increases as well.

In the second part, a parametric study of ladle design and argon flow rate on inclusion aggregation and removal has been conducted. Turbulence shear collision shows the most dominant effect on inclusion aggregation. The argon flow rate is positively related to inclusion aggregation and removal. When the argon flow rate is fixed, a larger plug separation angle shows higher inclusion aggregation and removal efficiency.

1 INTRODUCTION

The Ladle Furnace (LF) is part of the secondary steel making process. In the steel making process, the ladle receives the hot steel from a primary steel making process such as a Basic Oxygen Furnace (BOF) or Electric Arc Furnace (EAF) for transportation to the tundish to begin the casting process. Molten steel can also be heated, deoxidized, desulfurized, and alloyed in the ladle. Alongside temperature and composition homogenization of molten steel, inclusion removal also occurs in the ladle.

In the ladle, steel will be stirred by two main methods, they are gas-stirring and electromagnetic stirring (EMS). For gas-stirred ladles, two different gas injection method are used: bottom injection and top lance injection. In these, an inert gas such as argon or nitrogen will be injected from bottom porous plugs or top lances to stir the liquid steel. For EMS ladles, an external system of alternating current winding coils is used to generate a magnetic field to induce Lorentz forces in the conductive liquid metal and stir the fluid.

Because of the high temperatures and scale of ladle, it is difficult to directly measure the internal behaviors of an active ladle. There are two primary methods for investigating the behavior of ladle: physical experiments using fluids with similar observable physical behaviors and numerical modeling such as computational fluid dynamics (CFD). Continued development CFD models allows for increasingly accurate simulations of ladle physical phenomena enabling improved recreation and prediction of physical behavior.

In the thesis, flow characteristics and inclusion behavior including inclusion aggregation and removal in the bottom injection ladle will be studied.

1.1 Literature Review

There are two primary ways to study the flow phenomena occurring inside of ladle: physical experiments and numerical modeling based on computer analysis. For physical experiments, similar principle is a common method to translate the size and temperatures of a plant ladle into a lab size equivalent. Water modeling is a popular choice for study of the ladle flow field behaviors in a lab environment. For numerical modeling, powerful computational fluid dynamic simulation software such as ANSYS Fluent or STAR-CCM+ is used to simulate fluid flow characteristics.

Fluid behaviors may be modeled with continuous Eulerian field-based methods or with particle-based Lagrangian methods. Numerical modeling allows for exploration of operating conditions and ladle design factors including gas flow rate, slag thickness, plug distance ratio and plug separation angle, and more.

As for inclusion modeling, most of people use numerical method to simulate inclusion behavior. Inclusion can interact with neighbor inclusion and encounter bubbles, in these case, inclusion can aggregate to bigger size or take by bubbles and eventually be removed. For inclusion aggregation, there are four main methods: Brownian collision, turbulence shear collision, turbulence random collision and Stokes collision. In these four mechanism, inclusion Brownian collision only happened when inclusion size smaller than $1\mu m$.[1] For inclusion removal, there are 6 different removal mechanism: inclusion removal due to wall adhesion, slag absorption, inclusion-bubble interaction. And four different mechanisms are included in inclusion-bubble interaction: turbulence shear collision, turbulence random collision, Stokes collision and bubble wake capture.

1.1.1 Flow Characteristics in Ladle

In 1975, Szekely et al. [2] first modeled and studied the flow characteristic of ladle based on a simplified water model. Gas was injected from bottom, and bubble size was assumed as constant. All the boundary conditions were coming from physical measurement. By using Spalding's k-ω model, Navier-Stokes equation was solved in order to predict velocity and turbulence inside of water model. In 1978, DebRoy et al. [3] improved Szekely et al.'s model by revising bubble model from disperse bubbles constrained in single plume with diameter only related to volume fraction to injection gas flow rate.

Johansen et al. [4] adopted the experiments by using bottom injection water model. In his work, he found that the bubbles can created turbulence, and the turbulence will affect the flow velocity in bubble plume region. Peranandhantan et al. [5] conducted the experiment to find out expression of slag eye size in a simplified water model. Several variables such as gas flow rate, slag thickness, liquid depth and so on were test in the work. Top slag eye was capture and measured through camera. Mazumdar et al. [6] reviewed several studies on physical models and empirical correlation of gas-stirred ladle. Simplified expressions of several variables including gas flow rate, ladle dimensions and so on were well reviewed in his work.

Guo et al. [7] develop the 3-D simulation ladle using a Lagrangian-Eulerian model to predict gas-liquid two phase flow in the ladle. In this work, more detailed models such as lateral drag force and lift force and so on was added to predict plume shape. Plume spreading and mass transfer to rising bubble and top free surface are included. Zhang et al. [8] develop the Eulerian-Eulerian two phase flow system for ladle. Based on volume fraction difference, gas and liquid were considered as two continuous phase in one single space. K-ϵ was used to simulate turbulence inside of ladle. Lou et al. [9] developed a Eulerian-Eulerian numerical model to simulate gas-liquid two phase flow in the bottom injection gas-stirred system. The effect of turbulence dispersion force, drag force and lift force to flow field were studied. Bubble induced turbulence term was developed and written as source term in order to predict more accurate bubble plume shape. Cao et al. [10] detailed compare the difference between Eulerian-Eulerian method and Lagrangian-Eulerian method. In the work, Lagrangian-Eulerian method has more accurate results by both compared to experimental data.

1.1.2 Inclusion Behavior in Gas-Stirred Ladle

Normally, inclusions in the steel making process are considered as two different type: aluminum base and silicon base [11] , but most of studies were focus on aluminum base inclusion. For inclusion evolution, at the very beginning, aluminum ion will react with dissolved oxygen generate aluminum oxidation product, such as aluminum oxide (Al_2O_3). Then small oxide particles will nucleate, precipitate and grow to bigger size. When oxide particle grows big enough, they can collide and aggregate in the turbulence flow [12] . In order to distinguish these two phenomena, the change before collision will be called inclusion growth, after that will be called inclusion aggregation.

In this study, only inclusion aggregation will be considered. The behavior of inclusions consists of two parts: inclusion aggregation and inclusion removal. Lou et al. [1] conducted a review of all the inclusion behavior mechanism including inclusion aggregation and removal. In the past several decades, start from mid 1970s, people start to use numerical method to calculate and analyze inclusion behavior. In 1975, Szekely et al. [2] conduct a 2-D model to study inclusion aggregation by inclusion turbulence collision. In 1983, Shirabe.K et al. [13] also develop a 2-D model to predict inclusion aggregation by inclusion turbulence collision. What's more, he also studied inclusion

removal due to slag absorption. From 1986 to 1999, more and more people developed 2-D or 3-D model to simulate inclusion behaviors. [14, 15, 16, 17]

However, consideration of all the mechanisms including inclusion aggregation and inclusion removal were not studied together. In 2001, Mats Söder [18] talk about all the four mechanisms of inclusion aggregation and all three inclusion removal mechanisms. Four different bubble removal models were compared in his thesis. SÖder et al. [18] add more detailed regarding inclusion removal due to inclusion-bubble interaction. In this study, inclusion-bubble interaction including turbulence random collision, turbulence shear collision, laminar shear collision and stokes collision were considered.

In 2005, Wang et al. [19] reviewed inclusion removal process. The study proposed an expression of inclusion removal probability. The expression related to probability of adhesion, collision and detachment. In the study, author also mentioned that detachment so small that can be assume as zero. In 2013, Lou et al. [1] gave a more detailed inclusion behavior in the refining ladles. Three inclusion aggregation mechanisms and six inclusion removal mechanisms were conducted. Eulerian-Eulerian model was used to predict gas-fluid two phase flow, and bubble size was given. Standard k- ε turbulence model was employed to calculate turbulence behavior, and bubble induced turbulence was added as external source term into the model. For inclusion, in the study, Population Balance Model (PBM) was used to simulate inclusion size change. All the inclusions as continuum phase were divided into several groups based on their Sauter mean diameter.

1.2 Objective

The objective of the study is to use CFD to simulate inclusion behavior in a bottom injection gas-stirred ladle. The detailed objectives of the study are list below:

1) To develop a 3-D CFD simulation model to simulate the flow field inside of bottom injection ladle
2) To develop and validate inclusion behavior model with literature, and apply the method to a generic ladle
3) To analyze flow characteristics including flow field, slag eye size and wall shear stress in different ladles
4) To analyze inclusion aggregation behavior and removal process in different ladles.

2 METHODOLOGY AND CFD MODELS

2.1 Methodology of Inclusion Behavior in Gas-Stirred Ladle

Inclusion behavior modeling consists of two stages: flow simulation and inclusion simulation. Flow is first solved for a bottom injection gas-stirred system. The model includes three fluid phases: liquid steel, argon and slag. Argon gas is injected from two porous plugs at ladle bottom, interacting with these other phases as shown in Figure 1. After flow reaches a quasi-steady state, the flow results including turbulence kinetic energy, turbulence dissipation rate, pressure, velocity, and phase volume fraction are used in an inclusion-focused simulation as initial conditions via imported via interpolation.

In the inclusion simulation case, slag zone and argon zone (identified using volume fraction values) are set as solid domains, leaving only the liquid steel zone to be solved. Inclusions are treated as a new continuum phase in the liquid zone and be coupled with the Population Balance Model (PBM). The process is shown in Figure 2 below. The inclusion removal process relies on the use of coupled mass source terms. Because of the constant density of the inclusions, the reduction of mass are calculated as an inclusion phase volume fraction change. The inclusion removal rate (γ_i) is calculated based on following equation:

$$\gamma_i = \frac{\alpha_{i,\,t_0} - \alpha_{i,t}}{\alpha_{i,\,t_0}} \times 100\% \qquad (1)$$

$\alpha_{i,\,t_0}$ represents initial volume fraction of inclusion phase, and $\alpha_{i,t}$ is current volume fraction.

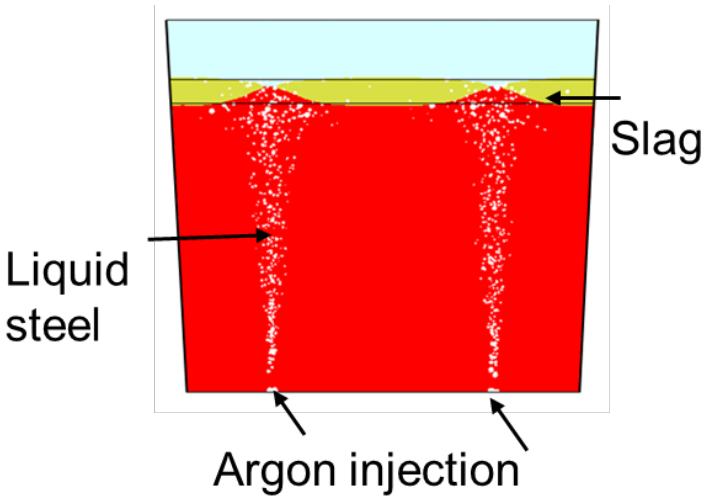

Figure 1. Schematic figure of gas-stirred ladle

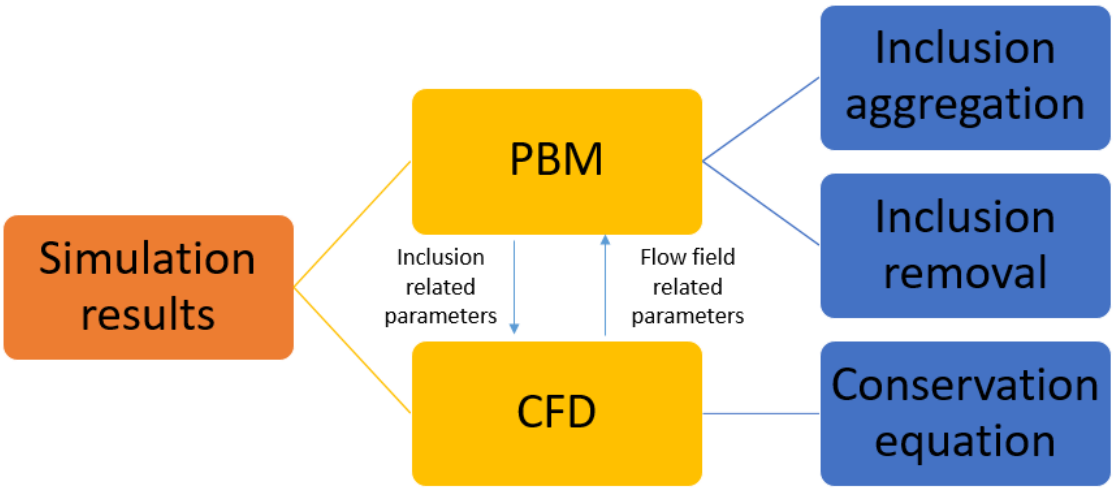

Figure 2. Overall simulation schematic

2.2 Assumptions of Inclusion Behavior in Gas-Stirred Ladle

The following assumptions are made for inclusion behavior in gas stirred ladle:

a. The steel in ladle is an incompressible Newtonian fluid, and turbulence flow is isotropic.
b. The flow is isothermal.

c. In first step, when flow is solved, the effect of slag on fluid flow will be accounted. In second step, only the shape of slag layer will be remained and the effect on inclusion behavior will be neglected.
d. The inclusion and bubble are assumed to be regular spheres. The inclusions are alumina.
e. The inclusions are initially evenly distributed in the ladle. Inclusion formation and growth are neglected, inclusion aggregation and inclusion removal are simulated.
f. Two smaller inclusions that collide can form a bigger size inclusion, but large size inclusions will never breakup to for smaller inclusions. Inclusion aggregation due to Brownian collision is not considered.
g. All inclusions that reach the steel-slag interphase will be ideally be absorbed by slag. There is no inclusion entrainment from the slag back to the steel.
h. The release of inclusions, which are carried by bubbles that burst at the slag eyes, back to the steel is not considered. The shape and size of slag eye are calculated from flow case.
i. A bubble that attaches to a bubble will never detaches.

2.3 CFD Models for Inclusion Behavior in Gas-Stirred Ladle

The inclusion behavior modeling consists of two different steps. The first step is to calculate the flow field and slag steel interface change as well as slag eye formation. The second step is to input the flow related parameters such as turbulence kinetic energy, turbulence dissipation rate, volume fraction of phases, pressure and velocity as initial condition and then to calculate inclusion behavior in gas-stirred ladle.

In the first step, in order to track flow field and argon bubble movement, VOF-Lagrangian model is used. The Volume of Fluid (VOF) model is used to simulate interphase behavior in three phases: steel, slag and argon. The Lagrangian (also called Discrete Phase model, or DPM) model is used to model bubble movement and behavior including bubble breakup and coalescence. In DPM model, virtual mass force, pressure gradient force and drag force are considered. Two-way turbulence coupling and discrete random walk model are employed to simulation turbulence influence by bubbles. For turbulence flow field, realizable $k - \varepsilon$ model is used.

In the second step, flow related parameters are applied as initial condition. In order to couple with PBM model, Eulerian-Lagrangian method is used. Eulerian-Eulerian multiphase model is employed to simulation interphase behavior between steel phase and inclusion phase. Slag phase

and argon phase are deactivated because only steel zone will be solved. Steel velocity are applied to inclusion, so inclusion will have the same velocity as steel. The volume fraction of slag phase and argon phase are only used to define the shape of slag layer. DPM model is used to simulate bubble behavior as well as inclusion bubble interaction. PBM model is used to simulate inclusion behavior including inclusion aggregation and inclusion removal. Inclusion size distribution will be solved by the model. Initial inclusion distribution can be calculated from equation (2), which adopted by Lou et al [1] :

$$n(d_j)_{t=0} = 2 \times 10^{14} \times e^{-d_j \times 10^6} \quad (2)$$

Eulerian - VOF Model Continuity Equation [21]

In flow simulation, VOF model is used to calculate multiphase interaction. Mass conservation can be express below:

$$\frac{\partial \rho}{\partial t} + \nabla \cdot (\rho \vec{u}) = S_m \quad (3)$$

In VOF model, all the phases will share one set of equation, so ρ here is the density of mixture, and $\vec{u}$ is local velocity. S_m is source term from m^{th} phase (steel, slag or argon).

Eulerian - VOF Model Momentum Equation [21]

For momentum conservation, the following equations will be applied:

$$\frac{\partial}{\partial t}(\rho \vec{u}) + \nabla \cdot (\rho \vec{u}\vec{u}) = -\nabla p + \nabla \cdot [\mu(\nabla \vec{u} + (\nabla \vec{u})^T)] + \rho \vec{g} + F_b \quad (4)$$

Where, p is local pressure, $\vec{g}$ represents local gravity acceleration, and F_b is the force from bubble.

Eulerian - Eulerian Model Continuity Equation [21]

For inclusion behavior simulation, Eulerian-Eulerian multiphase model is used to simulation steel and inclusion interface behavior, the general equation can be express below:

$$\frac{\partial}{\partial t}(\alpha_m \rho_m \vec{u}_m) + \nabla \cdot (\alpha_m \rho_m \vec{u}_m) = S_m \quad (5)$$

α_m represent phase volume fraction, ρ_m is phase density, and $\vec{u}_m$ is phase local velocity. For left side, S_m is source term from phase m (steel or inclusion).

Eulerian - Eulerian Model Momentum Equation [21]

$$\frac{\partial}{\partial t}(\alpha_m \rho_m \vec{u}_m) + \nabla \cdot (\alpha_m \rho_m \vec{u}_m \vec{u}_m) = -\alpha_m \nabla p + \nabla \cdot \bar{\bar{\tau}}_m + \alpha_m \rho_m \vec{g} + \vec{F}_{vm,m} \quad (6)$$

Where, $\bar{\bar{\tau}}_m$ represent phase m stress-strain tensor, $\vec{F}_{vm,m}$ is virtual mass force of phase m.

Turbulence Model [21]

In the simulation, for both flow simulation and inclusion behavior simulation, realizable k-ε model is used to model the turbulence field in the ladle. The following equations express the transport equation for turbulence kinetic energy (k) and turbulence dissipation rate (ε): [Fluent theory guide]

$$\frac{\partial}{\partial t}(\rho k) + \frac{\partial}{\partial x_m}(\rho k u_m) = \frac{\partial}{\partial x_n}\left[\left(\mu + \frac{\mu_t}{\sigma_k}\right)\frac{\partial k}{\partial x_n}\right] + G_k + G_b - \rho\varepsilon + S_k \quad (7)$$

$$\frac{\partial}{\partial t}(\rho \varepsilon) + \frac{\partial}{\partial x_m}(\rho \varepsilon u_i) = \frac{\partial}{\partial x_n}\left[\left(\mu + \frac{\mu_t}{\sigma_\varepsilon}\right)\frac{\partial \varepsilon}{\partial x_n}\right] - \rho C_1 S_\varepsilon - \rho C_2 \frac{\varepsilon^2}{k + \sqrt{v\varepsilon}} + C_{1\varepsilon}\frac{\varepsilon}{k} C_{3\varepsilon} G_b + S_\varepsilon \quad (8)$$

$$C_1 = \max\left[0.43, \frac{\emptyset}{\emptyset + 5}\right], \emptyset = S\frac{k}{\varepsilon}, S = \sqrt{2 S_{mn} S_{mn}} \quad (9)$$

Where, $C_{1\varepsilon}$ and C_2 are constant, G_k and G_b are the turbulence kinetic energy generation due to velocity gradient and buoyancy. S_k and S_ε represent source term to turbulence kinetic energy and turbulence dissipation rate. In this study, there is no turbulence related source term added. S is mean rate of strain tensor, which can be used to calculate C_1.

Discrete Phase Models [21]

Discrete Phase model is used to calculate inert gas bubble trajectory. It also provides a platform to calculate bubble breakup and coalescence model. Fluent calculate particle trajectory by calculating force balance of each particle. The force balance can be expressed below:

$$\frac{d\overrightarrow{u_p}}{dt} = F_D(\vec{u} - \vec{u}_p) + \frac{\vec{g}(\rho_p - \rho)}{\rho_p} + \overrightarrow{F_A} \quad (10)$$

In original version, subscript p represents tracked particle, in this study, p represent argon bubble. The first term $F_D(\vec{u} - \vec{u}_p)$ on left hand side is the drag force per unit particle mass, F_D can be expressed as:

$$F_D = \frac{18\mu}{\rho_p d_p^2}\frac{C_D Re}{24} \quad (11)$$

In this term, $\vec{u}$ is fluid phase velocity, and $\overrightarrow{u_p}$ is argon bubble velocity, Re is relative Reynolds number, can be expressed as:

$$R_e = \frac{\rho d_p |u - u_p|}{\mu_l} \quad (12)$$

C_D is drag coefficient, it can be express in several different ways, in the study, Hamathy's expression was chosen [20] :

$$C_D = \frac{2}{3}\left(\frac{E_0}{3}\right)^{0.5} \quad (13)$$

$$\mathrm{E_0} = \frac{g(\rho - \rho_p)d_p^2}{\sigma} \quad (14)$$

Where, $\mathrm{E_0}$ is the Eotvos number, it descript the relationship between buoyancy force and particle surface tension.

$\overrightarrow{F_A}$ represents additional force, virtual mass force $\vec{F}_{VM}$ one of them, it can expressed below:

$$\vec{F}_{VM} = -\frac{1}{2}\frac{\rho}{\rho_p}\left(\vec{u}_p \nabla\vec{u} - \frac{d\vec{u}_p}{dt}\right) \quad (15)$$

When $\rho > \rho_p$ an additional force due to pressure gradient will increase called pressure gradient force $F_{pressure}$and it can be expressed as:

$$F_{pressure} = \left(\frac{\rho}{\rho_p}\right)\overrightarrow{u_p}\nabla\vec{u} \quad (16)$$

As for gas density, it was calculated based on ideal gas law. The temperature for injection point is 1875 K.

Bubble Coalescence and Breakup Model

The bubble coalescence and breakup model is based on the theory proposed by Laux et al. [22] . In Laux et al.'s work, the bubble equilibrium diameter (d_b^e) can be calculated based on bubble surface tension (σ) and flow field turbulence dissipation rate (ε).

$$d_b^e = 4\alpha_b^{0.5}\frac{\left(\frac{\sigma}{\rho}\right)^{0.6}}{\varepsilon^{0.4}} + C_e \quad (17)$$

where, α_b is volume fraction of bubble, C_e refer as minimum bubble size from Pan et al [23] , in this study, minimum bubble size is 0.0001 m.

Relaxation time was employed to calculate bubble size change. The relaxation time represent the time needed for bubble change from current size to equilibrium diameter. When current bubble diameter smaller than equilibrium diameter, bubbles tend to coalescence to form bigger size bubbles; when current bubble diameter is bigger than equilibrium diameter, the bubbles tend to breakup to several smaller size bubbles. The Whole process can be expressed as:

$$\tau_{rel} = \begin{cases} \tau_B, & d_b > d_b^e \\ \tau_C, & d_b < d_b^e \end{cases} \quad (18)$$

Where, τ_{rel} represent relaxation time of bubble, τ_B represent bubble breakup timescale, and τ_C represent bubble coalescence timescale. τ_B and τ_C can be expressed as:

$$\tau_B = d_b^{\frac{2}{3}}\varepsilon^{-\frac{1}{3}} \quad (19)$$

$$\tau_C = 2\left[\frac{\pi\left(\alpha_{b,max} - \alpha_b\right)}{6\alpha_b}\right]^{\frac{1}{3}}\frac{d_b}{\sqrt{\frac{2}{3}k}}\sqrt{1 + \frac{\tau_b}{\tau_l}} \quad (20)$$

$$\tau_b = \sqrt{\left(\frac{\vartheta_l}{\varepsilon}\right)} \quad (21)$$

$$\tau_l = \frac{\rho_b d_b^2}{18\mu_l} \quad (22)$$

where, k is turbulence kinetic energy. τ_b and τ_l represent time scale of bubble relaxation and energetic turbulence eddies [21] , respectively. And ϑ and μ are the kinetic viscosity and dynamic viscosity of fluid phase.

In the turbulence flow, Laux et al. also restricted relaxation time by introducing turbulence microscale (τ_K):

$$\tau_{rel} = (\tau_{rel}, \tau_K)_{max} \quad (23)$$

$$\tau_K = 6\sqrt{\frac{\vartheta_l}{\varepsilon}} \quad (24)$$

For initial bubble size, this study takes average bubble diameter as initial bubble diameter. And the average bubble diameter can be assuming as 25% of maximum bubble diameter. Johansen et al. [24] proposed an equation to calculate maximum bubble diameter, and it can be express as:

$$d_{b,max} = 0.35\left({Q^2}/{g}\right)^{0.2} \quad (25)$$

where, Q is argon gas flow rate.

Population Balance Model [21]

Population balance model (PBM) is based on Population Balance Equation (PBE). In the study, only inclusion aggregation is considered. Inclusion growth and breakup will not be involved. The transportation equation for number density of particles can be express as:

$$\frac{\partial n(V_j,t)}{\partial t} + \nabla \cdot \left(\overrightarrow{u_p} n(V_j)\right) = \frac{1}{2}\int_0^{V_k} A(V_k - V_j, V_j) n(V_k - V_j, t) n(V_j, t)\,\mathrm{d}V_j - \int_0^{V_{max}} A\left(V_k, V_j\right) n(V_i, t)\,\mathrm{d}V_j + S_j \quad (26)$$

where, $n(V_j, t)$ is number density of j size inclusions. A represent aggregation rate of inclusion from size j to size k. S_j is external source term, it can be used to calculate inclusion removal.

Inclusion Aggregation Model

There are four main mechanisms are widely study in the world, they are Brownian motion aggregation, turbulence shear collision, turbulence random collision, and Stokes buoyancy collision. Brownian motion is mainly studied when inclusion size smaller than 1 μm; but in this study, smallest inclusion size is bigger than 1 μm. Thus, Brownian motion is not considered in this

study. Lou et al. [1] well reviewed the other three mechanisms. The overall inclusion aggregation rate is the summation of three mechanisms:

$$A_{jk} = A_{jk}^{TS} + A_{jk}^{TR} + A_{jk}^{S} \quad (27)$$

where, $A_{jk}^{TS}, A_{jk}^{TR}, A_{jk}^{S}$ represent inclusion aggregation rate from three mechanisms. j and k represent two different size of colliding inclusions.

1. Inclusion aggregation due to turbulence shear collision

In the turbulence flow field, smallest eddy size is called Kolmogorov microscale (K), it can be expressed as:

$$K = \left(\frac{\vartheta^3}{\varepsilon}\right)^{\frac{1}{4}} \quad (28)$$

When inclusion size is smaller than Kolmogorov microscale, this mechanism will be applied:

$$A_{jk}^{TS} = 1.294 E_{Shear}^{i-i} \left(\frac{\varepsilon}{\vartheta}\right)^{0.5} \left(r_j + r_k\right)^3 \quad (29)$$

$$E_{shear}^{i-i} = 0.732 \left(\frac{5}{N_T}\right)^{0.242} \quad (30)$$

$$N_T = \frac{6\pi\mu_l \left(r_j + r_k\right)^3 \left(\frac{4\varepsilon}{15\pi\vartheta_l}\right)^{0.5}}{8A_{isi}} \quad (31)$$

Where, E_{Shear}^{i-i} is capture efficiency of turbulence shear collision from two colliding inclusion. N_T is the force coefficient. A_{isi} is Hamaker constant and be assigned to 3.98×10^{19} J.

2. Inclusion aggregation due to turbulence random collision

When inclusion size is larger than Kolmogorov microscale, the intense turbulence in the flow field can drag inclusions in the bubbly plume region. But when inclusion size smaller than Kolmogorov microscale, the turbulence inertia effects can be applied. So the overall aggregation rate based on this mechanism can be express as:

$$d_1 = \min(d_j, d_k) \quad (32)$$

$$d_2 = \max(d_j, d_k) \quad (33)$$

For $d_1 \le K \le d_2$,

$$A_{jk}^{TR} = \frac{\pi}{2}(d_1 + d_2)^2 \left(d_2^{\frac{2}{3}} + K^{\frac{2}{3}}\right)^{\frac{1}{2}} \varepsilon^{\frac{1}{3}} \left(\frac{d_1}{K}\right)^3 \quad (34)$$

For $d_1 > K$,

$$A_{jk}^{TR} = \frac{\pi}{2}(d_1 + d_2)^2 \left(d_2^{\frac{2}{3}} + d_1^{\frac{2}{3}}\right)^{\frac{1}{2}} \varepsilon^{\frac{1}{3}} \quad (35)$$

For $d_2 < K$,

$$A_{jk}^{TR} = \frac{\pi}{2}(d_1 + d_2)^2 \sqrt{2} (\varepsilon K)^{\frac{1}{3}} \left(\frac{d_1 d_2}{K^2}\right)^3 \quad (36)$$

3. Inclusion aggregation due to Stokes buoyancy collision

Because of density difference, alumina inclusion can rise up. When inclusions rise up, the flow field can influence the inclusion rising path. The inclusion aggregation rate due to Stokes buoyancy collision can be expressed as:

$$A_{jk}^{S} = \frac{2g\pi(\rho_{\ l} - \rho_{\ i})}{9\mu_l} (r_j + r_k)^3 |r_j - r_k| E_{Stokes}^{i-i} \quad (37)$$

Where E_{Stokes} represents inclusion-inclusion stokes collision efficiency. Superscript i-i means inclusion-inclusion. The efficiency can be expressed as:

$$E_{Stokes} = E_{csu} \times sin^2\theta \times e^{\left\{3N_s\left[cos\theta\left(\ln\frac{3}{E_{csu}} - 1.8\right) - \frac{2+cos^3\theta - 3cos\theta}{2E_{csu}sin^2\theta}\right]\right\}} \quad (38)$$

$$E_{csu} = \min\left\{\left[\frac{-G}{1-G}\left(1+\frac{d_1}{d_2}\right)^2 + \frac{3d_1}{(1+G)d_2}\right], 1\right\} \quad (39)$$

$$G = \left(\frac{d_1}{d_2}\right)^2 \quad (40)$$

$$N_s = \frac{2u_{d_1}^S u_{d_2}^S}{g d_2} \quad (41)$$

$$u_p^S = \frac{g\left(\rho_{\ l} - \rho_{\ p}\right) d_p^2}{18\mu_l} \quad (42)$$

$$\beta = \frac{4E_{csu}}{9N_s} \quad (43)$$

$$\theta = \arcsin\{2\beta[(1+\beta^2)^{0.5} - \beta]\}^{0.5} \quad (44)$$

Where, E_{csu} is collision efficiency. N_s is Stokes number. u_p^S represents stokes velocity of rising particles, the particle can be inclusion or bubbles. θ represent colliding angle of two particles.

Inclusion Removal Model

There three different inclusion removal mechanisms: inclusion removal due to wall adhesion, inclusion removal due to slag absorption and inclusion removal due to bubble attachment. For bubble attachment, there are 4 different mechanisms: turbulence shear collision, turbulence random collision, bubble wake capture and buoyancy collision. For size j inclusion, the overall inclusion removal rate is summation of six mechanisms:

$$R_j = R_j^{wall} + R_j^{slag} + R_j^{TS} + R_j^{TR} + R_j^{wake} + R_j^{BF} \quad (45)$$

In the calculation, removal rate need to convert mass source so that it can be hook as mass source term into conservation equation.

$$S_j = \sum_{j=0}^{N-1} \rho_i V_j R_j \quad (46)$$

1. Inclusion removal due to wall adhesion

When inclusions move near the wall, some of them can be adhere to wall. The whole process control by fluid turbulence related parameter and fluid viscosity, the expression can be shown as:

$$R_j^{wall} = \frac{0.0062\varepsilon^{\frac{3}{4}}}{v^{\frac{5}{4}}} \frac{A_s}{V_{cell}} r_j^2 n(V_j, t) \quad (47)$$

Where, $n(V_j, t)$ represent current time size j inclusion number density, the unit for this is n/m^3. A_s and V_{cell} represent local slag cell effective area and volume.

2. Inclusion removal due to slag absorption

When inclusions move with flow field near the slag layer, they can be capture by slag because of their own Stokes floating and turbulence fluctuation. The whole expression can be shown as:

$$R_j^{slag} = \left(u_j^S + \frac{u_j^T}{6}\right) \frac{A_s}{V_{cell}} n(V_j, t) \quad (48)$$

$$u_j^T = 1.4(\varepsilon d_j)^{\frac{1}{3}} \quad (49)$$

Where u_j^T represents turbulence velocity.

3. Inclusion removal due to turbulence shear collision

Similar to inclusion aggregation mechanism, when bubble size smaller than eddies size, the mechanism can be applied. The removal rate can be express as:

$$R_j^{TS} = 1.294 E_{shear}^{i-b} \left(\frac{\varepsilon}{v}\right)^{0.5} (r_j + r_b)^3 \frac{6\alpha_b}{\pi d_b^3} n(V_j, t) \quad (50)$$

$$E_{shear}^{i-b} = 0.732\left(\frac{5}{N_T}\right)^{0.242} \quad (51)$$

$$N_T = \frac{6\pi\mu_l\left(r_j + r_b\right)^3\left(\frac{4\varepsilon}{15\pi\nu_l}\right)^{0.5}}{8A_{isb}} \quad (52)$$

Where, E_{shear}^{i-b} is capture efficiency between bubble and inclusion. A_{isb} is Hamaker constant assigned to 6.47×10^{19} J for inclusion-bubble collision.

4. Inclusion removal due to turbulence random collision

Similar to inclusion aggregation mechanism, especially when inclusion size greater than Kolmogorov microscale, the inclusion can be drag by turbulence eddy. This is an important cause of inclusion–bubble collision and result in inclusion attached to bubbles. The removal rate caused by inclusion-bubble random collision can be expressed as:

For $d_j > K$

$$R_j^{TR} = C\frac{\pi}{4}\left(d_j + d_b\right)^2\left(\varepsilon d_j\right)^{\frac{1}{3}}\frac{6\alpha_b}{\pi d_b^3}n\left(V_j, t\right) \quad (53)$$

For $d_j \leq K$

$$R_j^{TR} = C\frac{\pi}{4}\left(d_j + d_b\right)^2\left(\varepsilon K\right)^{\frac{1}{3}}\left(\frac{d_j}{K}\right)^3\frac{6\alpha_b}{\pi d_b^3}n\left(V_j, t\right) \quad (54)$$

Where, C is a constant, assume 2 here.

5. Inclusion removal due to bubble wake capture

The bubble wake capture only happens near the slag-steel interface. When inclusion at slag-steel, it can be drag by bubble wake moving together and eventually removed by slag. The inclusion removal based on this phenomenon can be expressed as:

$$R_j^{Wake} = 3.45\alpha_b\left(u_b + u_l\right)\frac{A_s}{V_{cell}}n\left(V_j, t\right) \quad (55)$$

6. Inclusion removal due to buoyancy collision

Due to the rising velocity difference between bubble and inclusion, inclusion can be captured by bubbles. The colliding angle can influent collision efficiency. The inclusion removal due to buoyancy collision can be expressed as:

$$R_j^{BF} = \frac{\pi}{4}\left(\mathrm{d}_j + \mathrm{d}_b\right)^2 (u_b - u_i)\frac{6\alpha_b}{\pi d_b^3} n\left(V_j, t\right) E_{Stokes}^{b-i} \quad (56)$$

Where, E_{Stokes}^{b-i} represent collision efficiency, it can be calculate based on angle of two colliding particles (shown in inclusion aggregation part). The superscript b-i means colliding particles are bubble and inclusion.

3 RESULTS AND DISCUSSION

3.1 Computational Geometry and Mesh

In this section, the geometry and mesh of full-scale ladle model and inclusion validation ladle model will be shown. The full-scale ladle model is developed based on a two-plug ladle owned by Nucor Steel. The geometry has been simplified. This geometry will be used to simulation and compare the results from flow field and inclusion removal. The validation ladle model is developed based on Lou et al. [1] This geometry is used to validate inclusion aggregation and removal model.

3.1.1 Full-Scale Bottom Injection Ladle Model

The full-scale simulation ladle was developed, with simplification made, based on a two-plug ladle owned by Nucor Steel. There are two plugs located at bottom. In this study, two different design of ladle were build: one is plug separation angle of 180°, another is plug separation angle of 90°. The geometries are shown below:

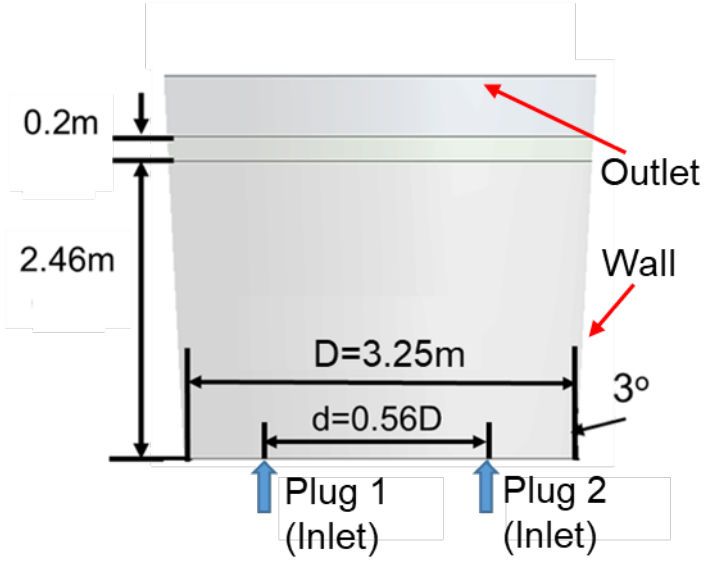

Figure 3. Separation angle of 180° ladle simplified geometry

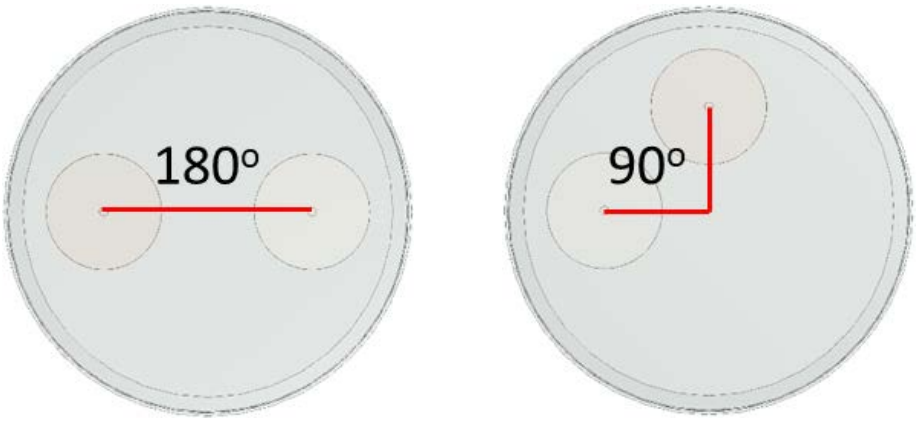

(a) (b)

Figure 4. Plug separation angle schematic figure: (a) Plug separation angle of 180°; (b) Plug separation angle of 90°

Because of the purpose of simulation, finer mesh near the boundary is needed to capture the force and inclusion volume fraction gradient. The total mesh cell for both geometries is around 3.5 million.

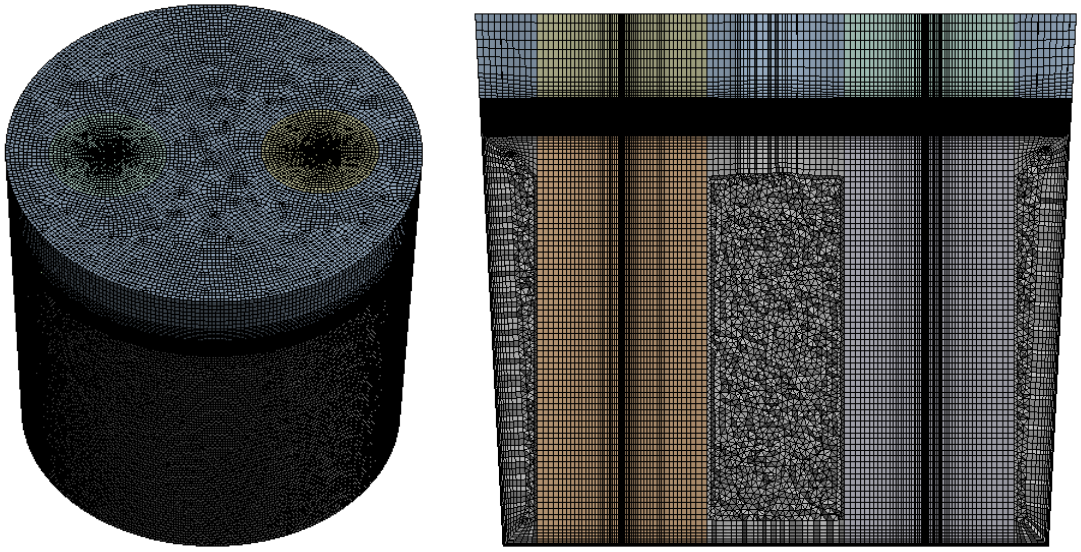

(a) (b)

Figure 5. Mesh for separation angle of 180° ladle: (a) Front view;
(b) Center-cut section plane view

3.1.2 Validation inclusion aggregation and removal ladle model

Inclusion removal validation geometry were adopted based on Lou et al.'s work [1]. The upper ladle diameter is 3115mm and the lower ladle diameter is 2578 mm. The height of ladle is 3200 mm. In this work, flat free surface was assuming for top slag-steel interface. The slag zone was not be simulated. But a slag eye area was assumed at top. The slag eye area can be calculated based on mathematical model adopted by Krishnapisharody et al, 2008 [26]. The detailed equation has been listed below:

$$\frac{A_e}{H^2} = -0.76\left(\frac{Q_g}{g^{0.5}H^{2.5}}\right)^{0.4} + 7.15\left(1-\frac{\rho_s}{\rho_l}\right)^{-0.5}\left(\frac{Q_g}{g^{0.5}H^{2.5}}\right)^{0.73}\left(\frac{h}{H}\right)^{-0.5} \quad (57)$$

Where, A_e represent slag eye area, H and h are the ladle height and slag thickness. Q_g is gas flow rate in m^3/s. ρ_s and ρ_l are slag density and liquid steel density, respectively. Slag thickness and density have not been listed in this work, but can be referred from Lou et al. [25]. Here, slag thickness is 95 mm, slag density is 3000 kg/m^3. Gas flow rate is 200 NL/min. Substitute numbers into equation, the slag eye area can be calculated which is 0.3146 m^3.

The wall and slag have been refined in order to capture high velocity and turbulence dissipation rate gradient near the wall. Figure 6 below geometry of validation ladle.

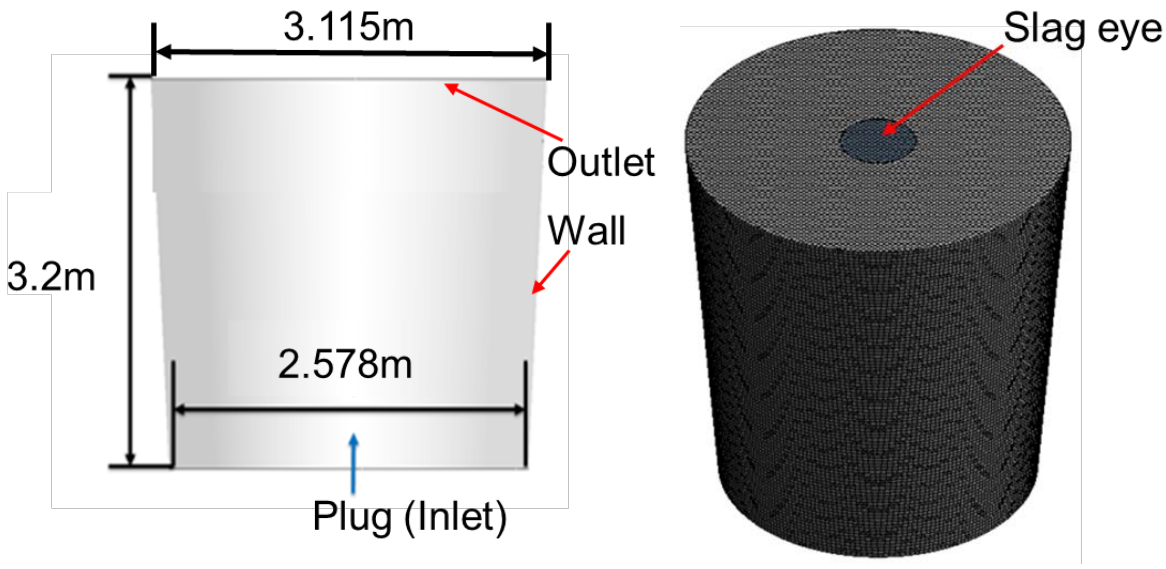

(a) (b)

Figure 6. Validation ladle geometry and mesh: (a) Geometry front view; (b) Mesh

3.2 Boundary conditions

3.2.1 Boundary conditions for full-scale ladle flow simulation

Inlet: For 180° ladle, the flow rate for both plugs are 5 SCFM. For 90° ladle, three different flow rate combination were studied: 1). 5 SCFM and 5 SCFM; 2). 5 SCFM and 20 SCFM; 3). 20 SCFM and 20 SCFM.

Outlet: For both design of ladle, outlet was set as pressure outlet.

Wall: Wall boundary conditions for both ladle designs was set as an insulting wall. Because of the purpose of simulation, the enhanced wall function was used to calculate wall shear stress.

3.2.2 Boundary condition for full-scale ladle inclusion behavior simulation

As mentioned before, after flow reach the quasi-steady state the flow results are used to perform the inclusion study using the “frozen” flow field wherein the slag zone and air zone will be converted to numerical solids.

Inlet: The inlet will keep the same boundary condition as flow simulation case.

Outlet: The original outlet is located at solid zone, so pressure outlet will be changed to wall. Actually, the slag – steel interface will be considered as new outlet. The boundary condition for DPM model is set as escape.

Wall: same as flow simulation.

Inclusion: by using PBM model, the inclusion will be divided into 11 groups from 5 μm to 50 μm. The initial size distribution can be calculated based on Equation (2). Table 1 shows detailed initial size distribution of full-scale ladle.

Table 1. Inclusion size volume fraction distribution at 0 seconds

Size (μm)	Volume fraction
5.0	55.0%
6.3	30.0%
7.9	11.0%
10.0	4.0%
12.7	0.0%
16.0	
20.0	
25.4	
32.0	
40.3	
50.8	

3.2.3 Boundary condition for inclusion behavior validation ladle

Inlet: 200NL/min argon gas will be injected from inlet plug. The Discrete Phase Model (DPM) is used to predict bubble move trajectory. Bubble size is assumed as a constant 0.004 m.

Outlet: Top surface is assumed as flat free surface. All the bubble will escape from top surface.

Wall: Side wall is assumed as no slip solid wall.

Inclusion: Inclusion size is assumed from 4 μm to 200 μm divided into 18 groups. The initial size distribution can be calculated from Equation (2). Initially, mainly small size inclusion will be distributed in the ladle.

3.3 Flow characteristics analyze

The slag eye size is chosen to validate simulation results with real plant measurement. The real plant measurement is based on Nucor Decatur separation angle of 180° ladle, flow rate is 30 SCFM for both plugs. The measured slag eye size is 0.73 m (mean diameter for both slag eye area), CFD simulation shows the mean diameter of two slag eye is 0.79 m. The overall error is 7.5% which is less than 10%. In this study, by using same models, the slag eye size, wall shear stress and flow field will be compared.

3.3.1 Bubble size distribution

Bubbles are injected from the bottom of the ladle by using the DPM model. During travel, a bubble can breakup into several smaller sized bubbles or coalesce with another bubble to form a bigger bubble depending on the equilibrium bubble diameter. The bubble size distribution along the ladle vertical axis for separation angle of 180° with gas flow rate for both plugs of 5 SCFM is shown in Figure 7. Because of lower pressure, larger bubbles are found towards the top region of ladle. From Figure 8, three layers of depth in the ladle are used to quantify the bubble size distribution. As shown in Figure 9, most layers have a bubble diameter of around 0.01m which is greater than the initial bubble size. Table 2 shows initial and maximum bubble diameter for four cases. As flow rate increases, maximum bubble size will increase.

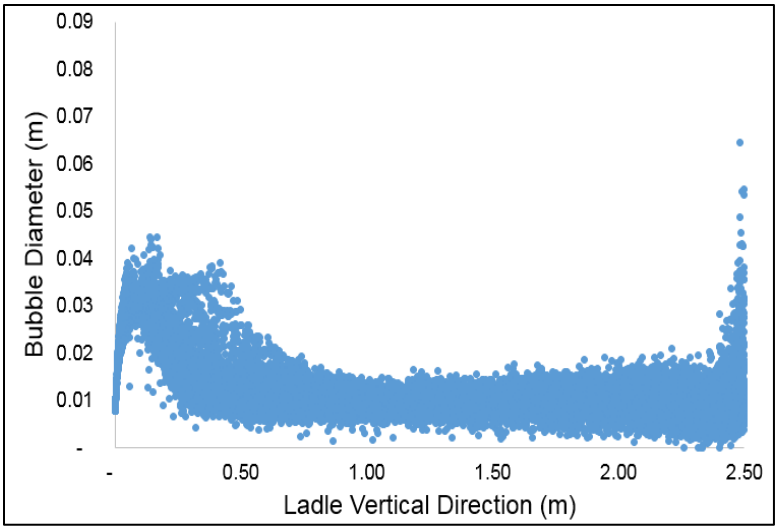

Figure 7. Bubble size distribution in whole domain

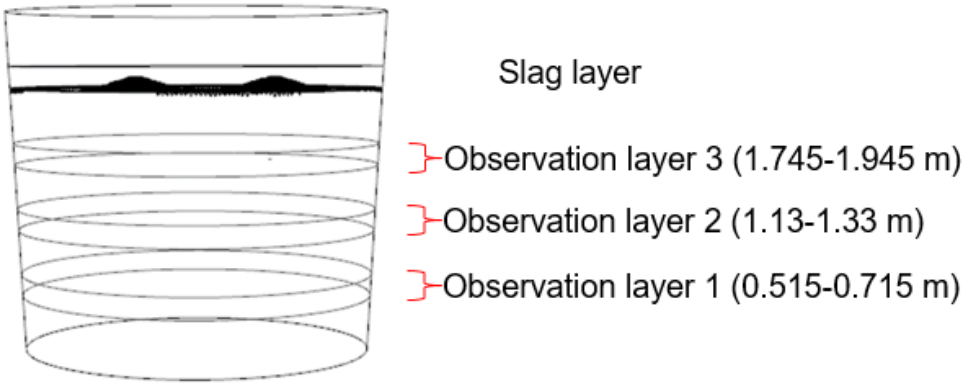

Figure 8. Bubble size distribution observation layers

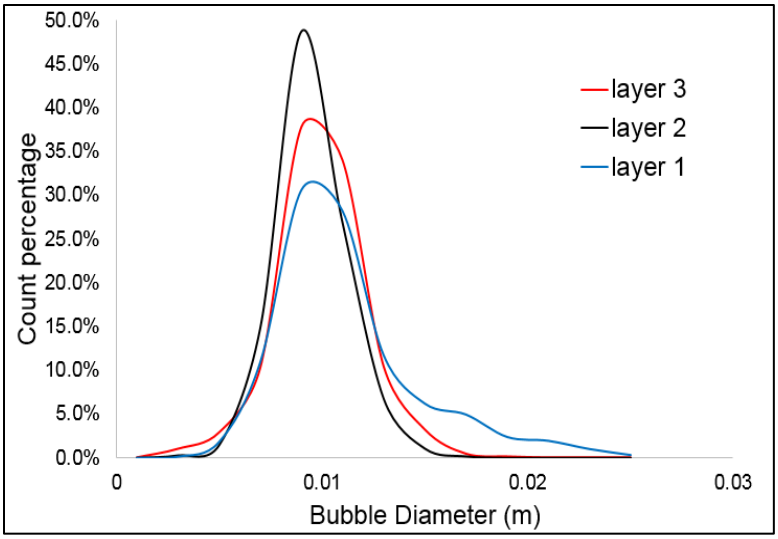

Figure 9. Bubble size distribution in three observation layers

Table 2. Initial and maximum bubble diameter for different cases

Case	Initial bubble diameter (m)	Maximum Bubble diameter (m)
Case 1 (180° 5/5 SCFM)	0.0067	0.0608
Case 2 (90° 5/5 SCFM)	0.0067	0.0620
Case 3 (90° 5/20 SCFM)	0.0067, 0.0117	0.1102
Case 4 (90° 20/20 SCFM)	0.0117	0.1089

3.3.2 Flow field

Due to the different plug position, different cross sectional planes have been created for 180° and 90° ladle respectively. As shown in Figure 10, plane 1 and 2 through the plugs perpendicular to the bottom of the ladle; plane 3 and 4 located center of the ladle and cross plane 1 and 2 at a 90° angle.

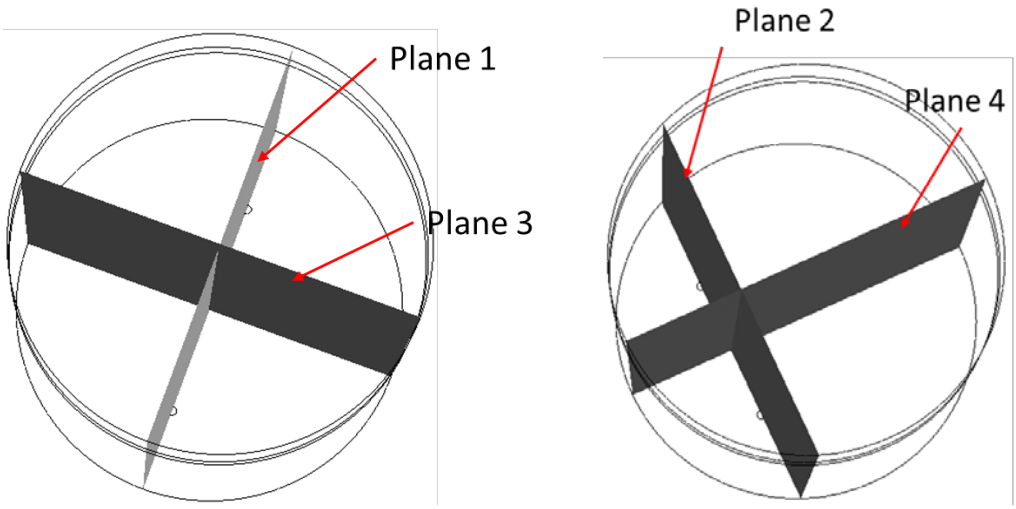

(a) (b)

Figure 10. Cross sectional plane for two ladle geometry: (a) Separation angle of 180° ladle; (b) Separation angle of 90° ladle

A velocity vector based on these planes is shown in Figure 11 and Figure 12. The highest velocity appears at the plume region, because the liquid steel will be entrained by the rising gas bubbles. As shown in planes 1 and 2, around two plume regions, circulations are formed. However, there is some difference between planes 3 and 4. For the 180° ladle, there are two flow circulations which meet at the center of the plane. For the 90° ladle, two flow circulations meet at the center of two plumes. In general, there is always a tendency for molten steel to move to the center of the two gas plumes, and the dead zones can always be found at the corner of ladle.

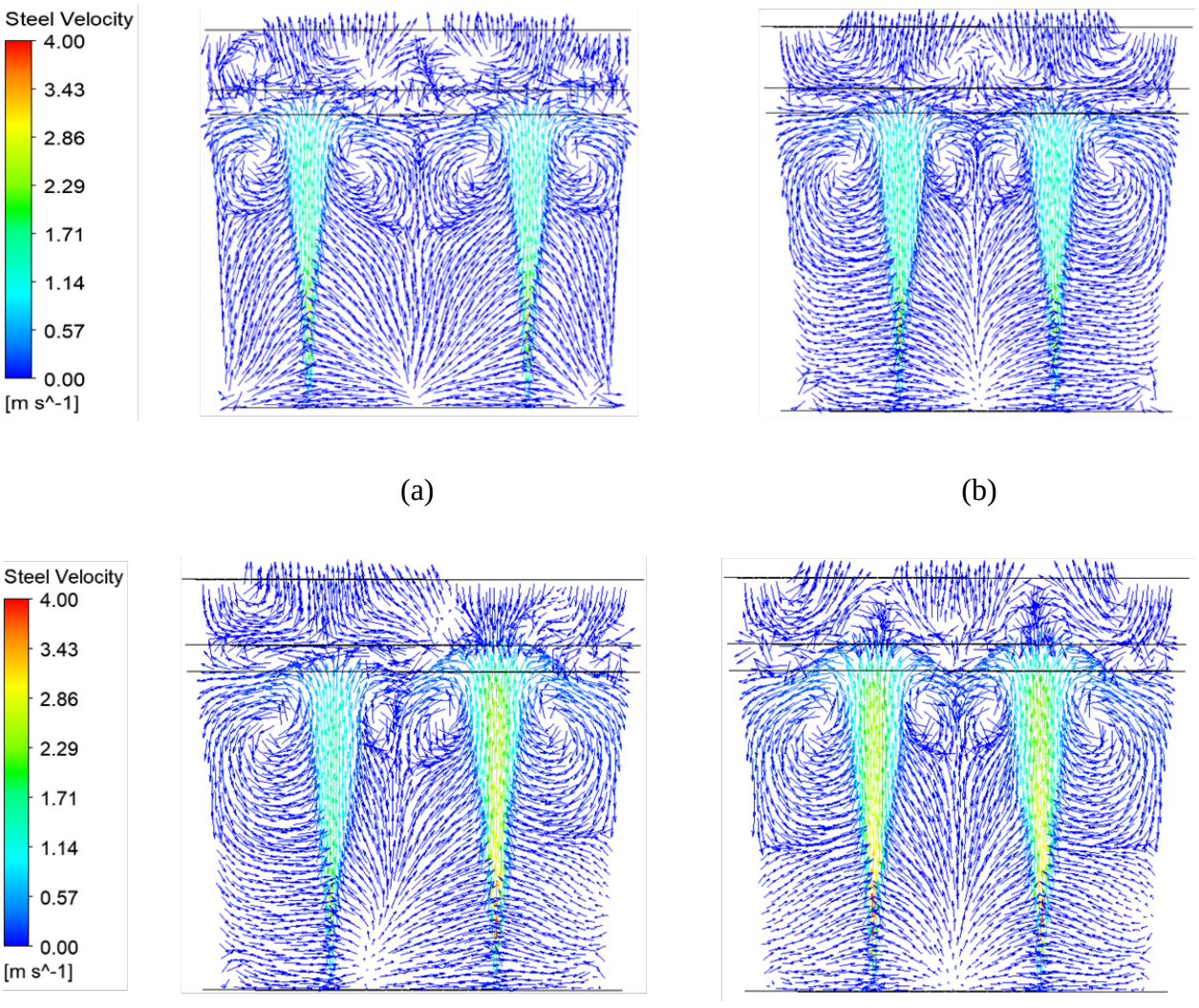

Figure 11. Flow velocity vector in plug cross-section plane: (a) 180° 5/5 SCFM, plane 1; (b) 90° 5/5 SCFM, plane 2; (c) 90° 5/20 SCFM, plane 2; (d) 90° 20/20 SCFM, plane 2.

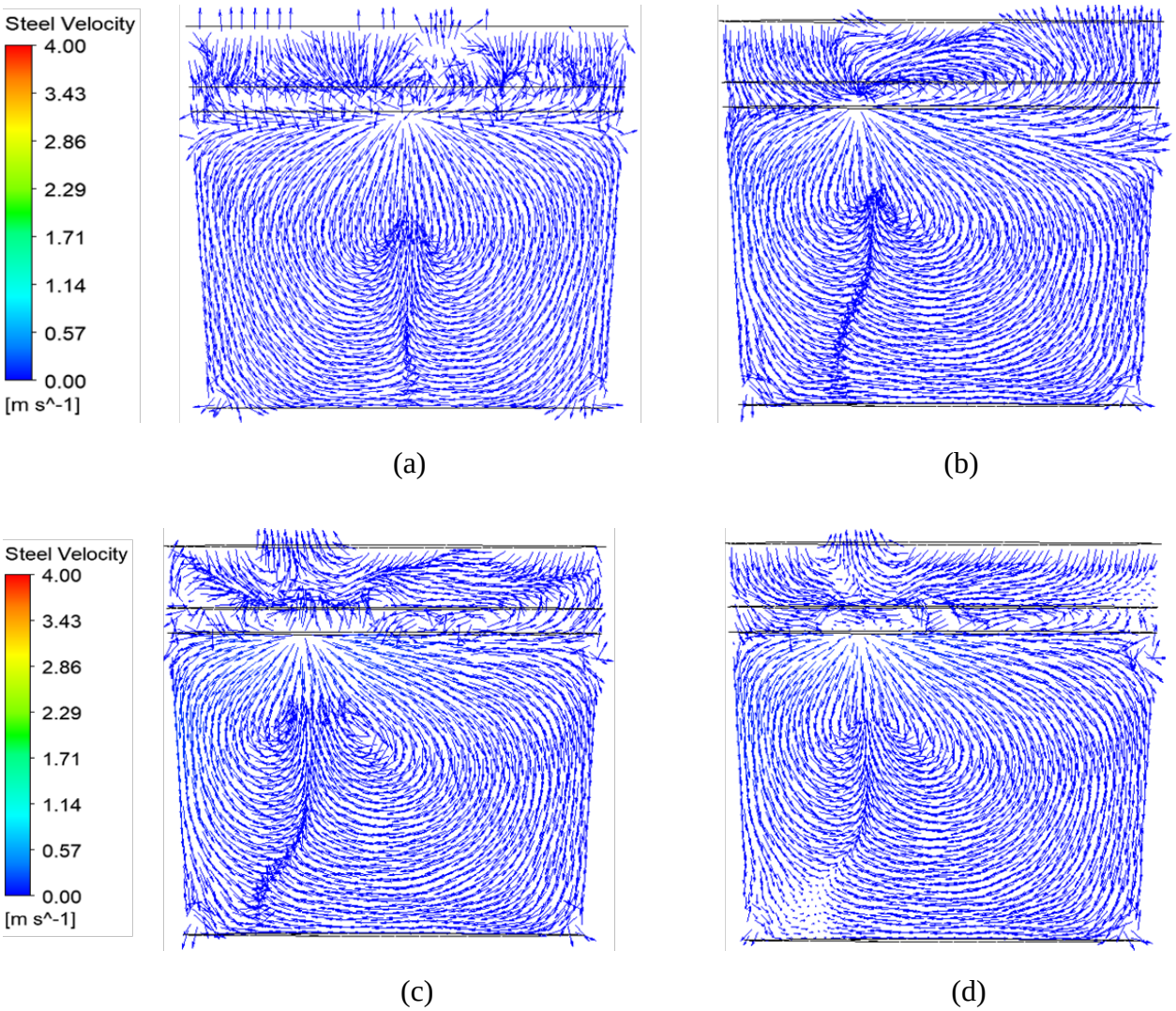

Figure 12. Flow velocity vector in center plane: (a) 180° 5/5 SCFM, plane 3; (b) 90° 5/5 SCFM, plane 4; (c) 90° 5/20 SCFM, plane 4; (d) 90° 20/20 SCFM, plane 4.

3.3.3 Slag eye size

Slag eye size is a very important factor to control steel cleanliness during the steel refining process in ladle. Normally, slag eye size has a positive correlation with the gas flow rate, but sometimes the ladle geometry can also affect the size of slag eye. In this study, slag eye size has been measured with 180° and 90° under different argon gas flow rate. As shown in Figure 13, under an argon flow rate of 5 SCFM for both plugs, whether at 180° or 90° ladle, there is no slag eye. When the plug separation angle is fixed, increasing argon gas flow rate, the slag eye size will increase as shown in Figure 13. Table 3 shows the mean diameter of slag eye for all different cases. From the table, two plugs with different flow rates can result in slightly larger slag eye size.

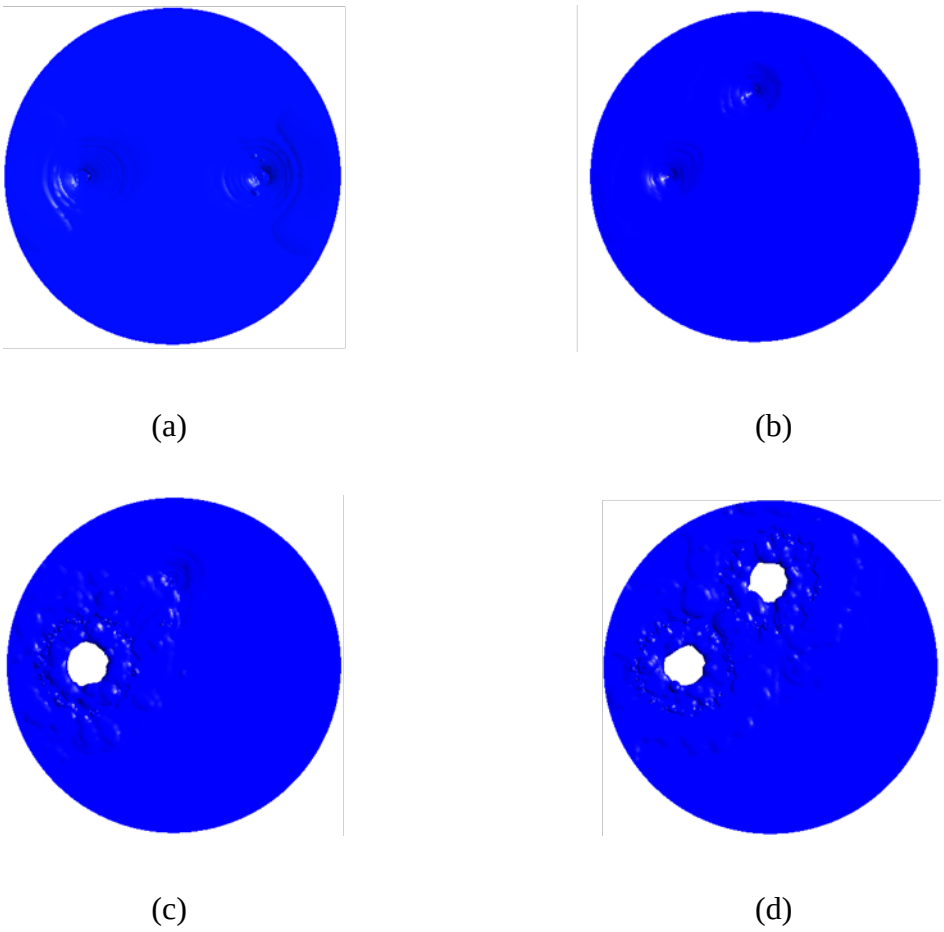

(a) (b)

(c) (d)

Figure 13. Slag eye size and shape for different cases: (a) 180° 5/5 SCFM; (b) 90° 5/5 SCFM; (c) 90° 5/20 SCFM; (d) 90° 20/20 SCFM.

Table 3. Mean diameter of slag eye for different cases

Case	Slag eye diameter (m)
Case 1 (180° 5/5 SCFM)	0
Case 2 (90° 5/5 SCFM)	0
Case 3 (90° 5/20 SCFM)	0.64
Case 4 (90° 20/20 SCFM)	0.62

3.3.4 Wall Shear Stress

Wall shear stress is an important factor to predict ladle refractory wall service lifetime. Wall shear stress will be different from one ladle design to another. It is important to find out the higher region of shear stress around the ladle wall. Usually, higher wall shear stress will appear near the argon

gas plume. As shown in Figure 14, all cases have the same trend of higher wall shear stress being located at the upper part of ladle near the gas plume. This is because the steel flows with argon gas to the slag-steel interface and then attaches to the wall creating circulation, as shown in Figure 11. Comparing Figure 14 (b), (c) and (d), it is easy to recognize when the gas flow rate increase, the wall shear stress will increase as well. Table 4 shows the maximum wall shear stress for all four different cases. When the gas flow rate is fixed, if the two plugs position is closer, maximum wall shear stress will increase. But when the plug position is fixed, the maximum wall shear stress is mainly affected by the argon gas flow rate.

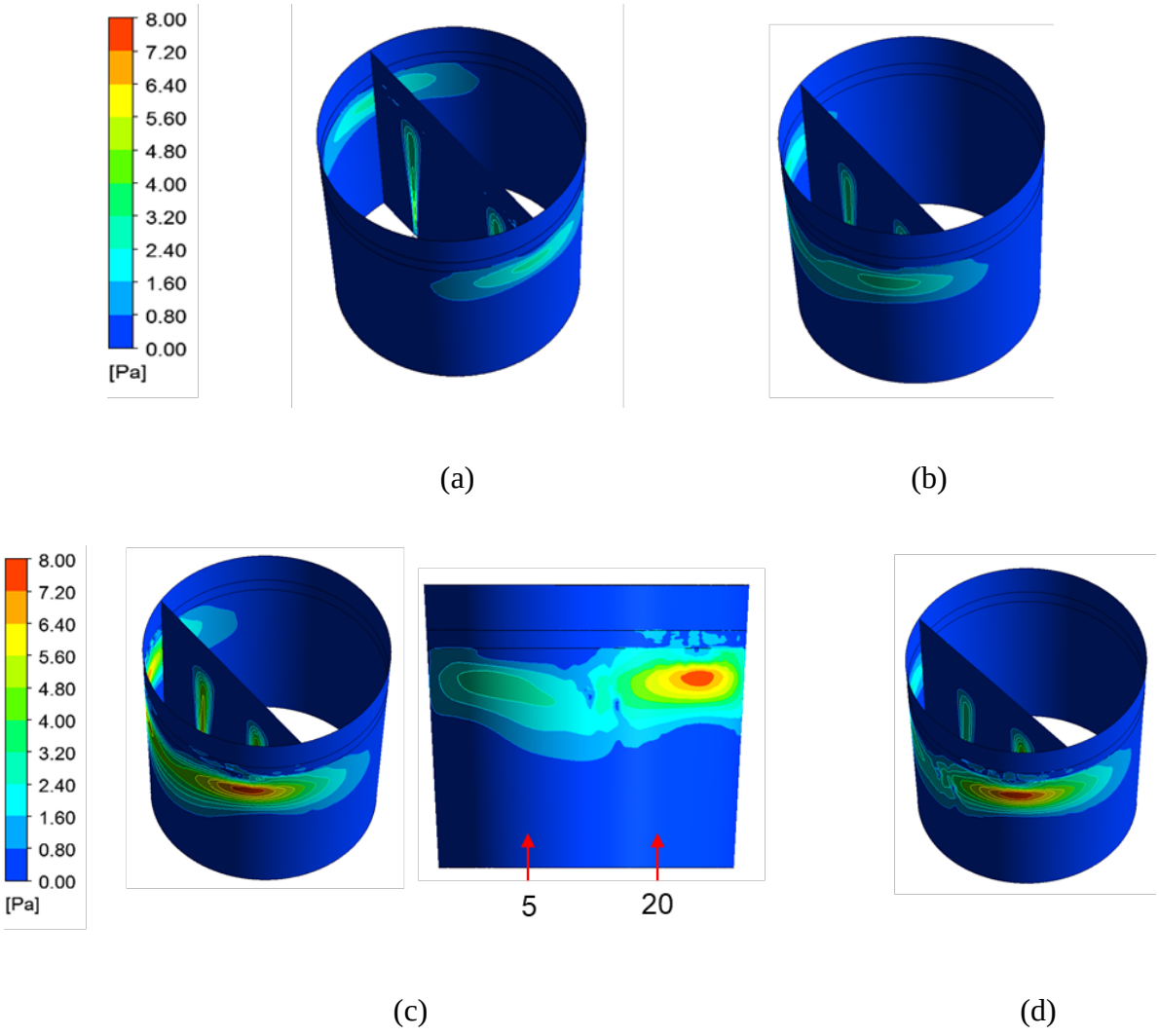

Figure 14. Wall shear stress contour for different cases: (a) 180° 5/5 SCFM; (b) 90° 5/5 SCFM; (c) 90° 5/20 SCFM; (d) 90° 20/20 SCFM

Table 4. Maximum wall shear stress for all cases

Case	Maximum wall shear stress (Pa)
Case 1 (180° 5/5 SCFM)	2.71
Case 2 (90° 5/5 SCFM)	2.82
Case 3 (90° 5/20 SCFM)	8.07
Case 4 (90° 20/20 SCFM)	8.07

3.4 Inclusion Behavior Analysis

3.4.1 Validation

For the modeling of the inclusion removal process, inclusions are only removed by interaction with the slag and walls. The bubbles serve as transportation for moving the inclusions to the slag steel interface. At the interface, if a bubble breaks up at the slag area, all the inclusions will be removed by the slag; if bubbles breakup at the slag eye area, inclusions will be released back into steel. In the current simulations, inclusion release back from the slag eye is not modeled, as inclusions captured by bubbles are considered to be removed immediately. Therefore, the current models over-predict the overall inclusion removal rate compared to the study being used for validation (which does model inclusion re-release).

In this simulation, overall removal rate is 98.6%. Table 6 shows the relative contribution from different mechanisms. From the data, the most dominant removal mechanism is bubble capture. However, 29.27% of the bubbles rupture at slag eye area as shown in Table 5. With the assumption that all inclusion capture by bubbles that burst at the slag eye are then re-release back into steel, 29.27%inclusion removed by bubble can therefore be considered as re-released into the steel. With this assumption, the overall removal rate drops to 69.53%, which is similar to the 68.16% reported by Lou et al.

Table 5. Bubble rupture position statistics percentage

	Slag area	Slag eye area
Mass percentage	70.23%	29.27%

Table 6. Removal mechanisms contribution in validation ladle

	Slag	Wall	Bubble
Removal Rate	1.90%	0.001%	98.1%

Table 7. Inclusion removal rate

	Overall	Overall (consider bubble rupture at slag eye)	Lou et al, 2013
Removal rate	98.6%	69.9%	68.16%

3.4.2 Inclusion Aggregation in Full Scale Ladle

Inclusion aggregation rate is the summation of three different mechanisms: inclusion aggregate due turbulence shear collision, inclusion aggregate due to turbulence random collision and inclusion aggregate due to stokes collision. In order to find out which mechanisms is more dominant during the inclusion aggregation process, without considering inclusion removal mechanisms, several simulations had been studied. Figure 15 shows the importance mechanisms in 180° ladle, 5 SCFM gas flow rate for both plugs at 300 seconds. In the figure, the less big size inclusion, the more important the missing mechanism. So it is easy to find that turbulence shear

collision is most dominant mechanism among three aggregation mechanisms. After turbulence shear collision are stokes collision and turbulence random collision.

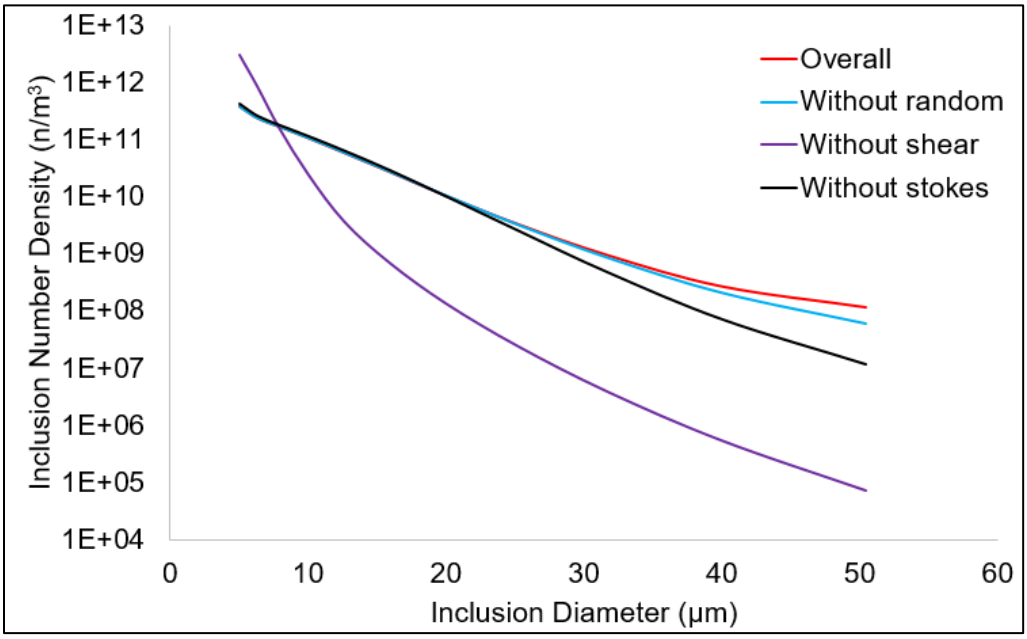

Figure 15. Importance of inclusion aggregation mechanisms comparison at 300 seconds in 180° ladle, 5/5 SCFM

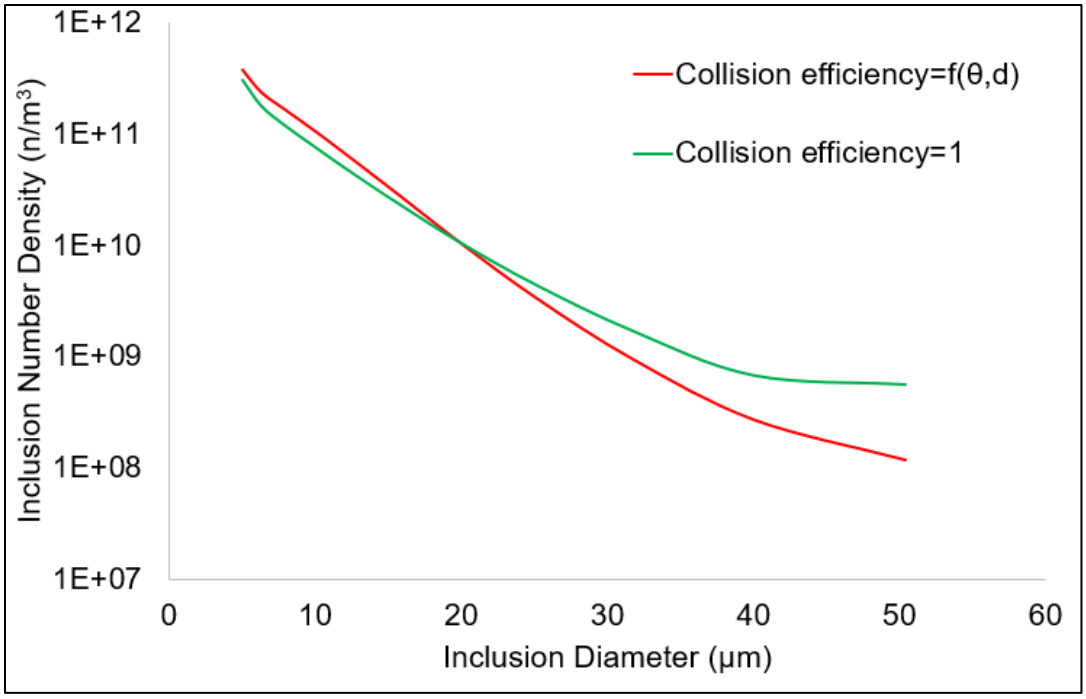

Figure 16. Effect of stokes collision efficiency on inclusion aggregation at 300 seconds in 180° ladle, 5/5 SCFM

For Stokes collision, there is an important factor called Stokes collision efficiency. Figure 16 shows inclusion aggregation in a 180° plug separation ladle with a calculated Stokes efficiency and without (ie. Stokes efficiency is assumed to be 100%). When not considering the efficiency value, a greater quantity of large inclusions aggregate. When the collision efficiency is assumed 100% in a case with no inclusion removal, the fully-developed number density is 7.7×10^{11} per cubic meter. However, when the calculated Stokes efficiency is used the inclusion number density is 9.9×10^{11} per cubic meter. There is 22.2% difference in total number of inclusions due to smaller inclusions aggregating (thus reducing the number). The magnitude of this effect means that collision efficiency must be considered in inclusion aggregation calculation.

Figure 17 shows four different cases inclusion size volume fraction distribution due to aggregation mechanisms only. It is easy to find that when plug position is fixed, increase in argon flow rate can result in higher inclusion aggregation rate; when argon flow rate is fixed, 180° ladle shows higher aggregation rate than 90° ladle.

Turbulence dissipation rate is found to be positively related to inclusion aggregation and removal. Figure 18 shows the turbulence dissipation rate in ladles. Table 8 gives an idea that the volume average turbulence dissipation rate in different design or flow rate of ladles.

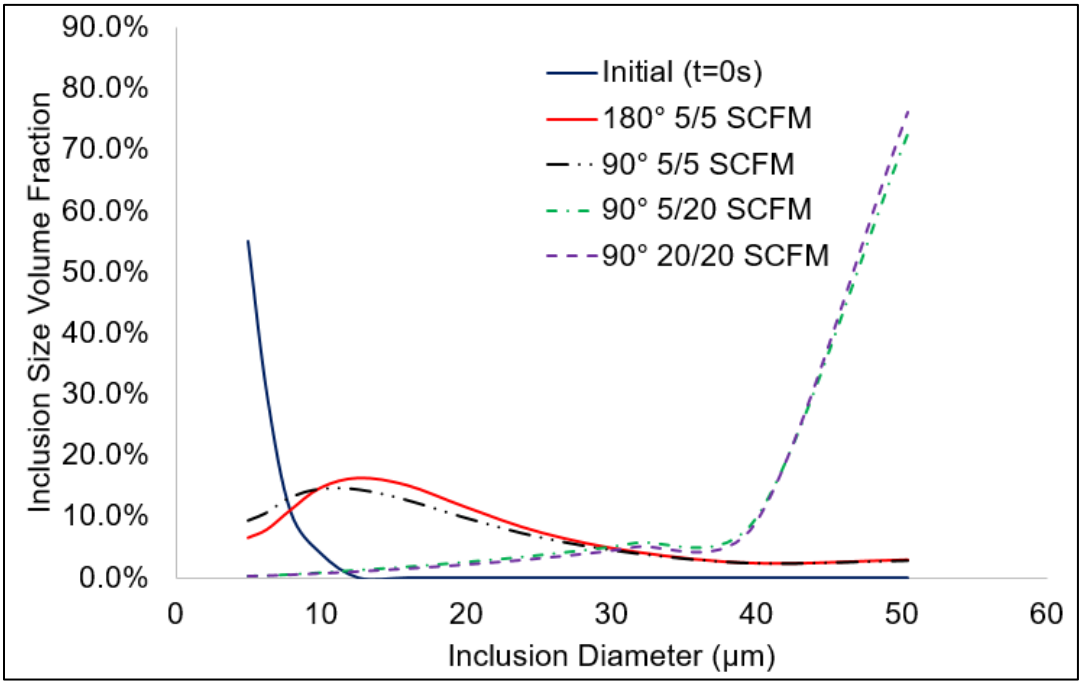

Figure 17. Inclusion size volume fraction distribution in different cases at 300 seconds

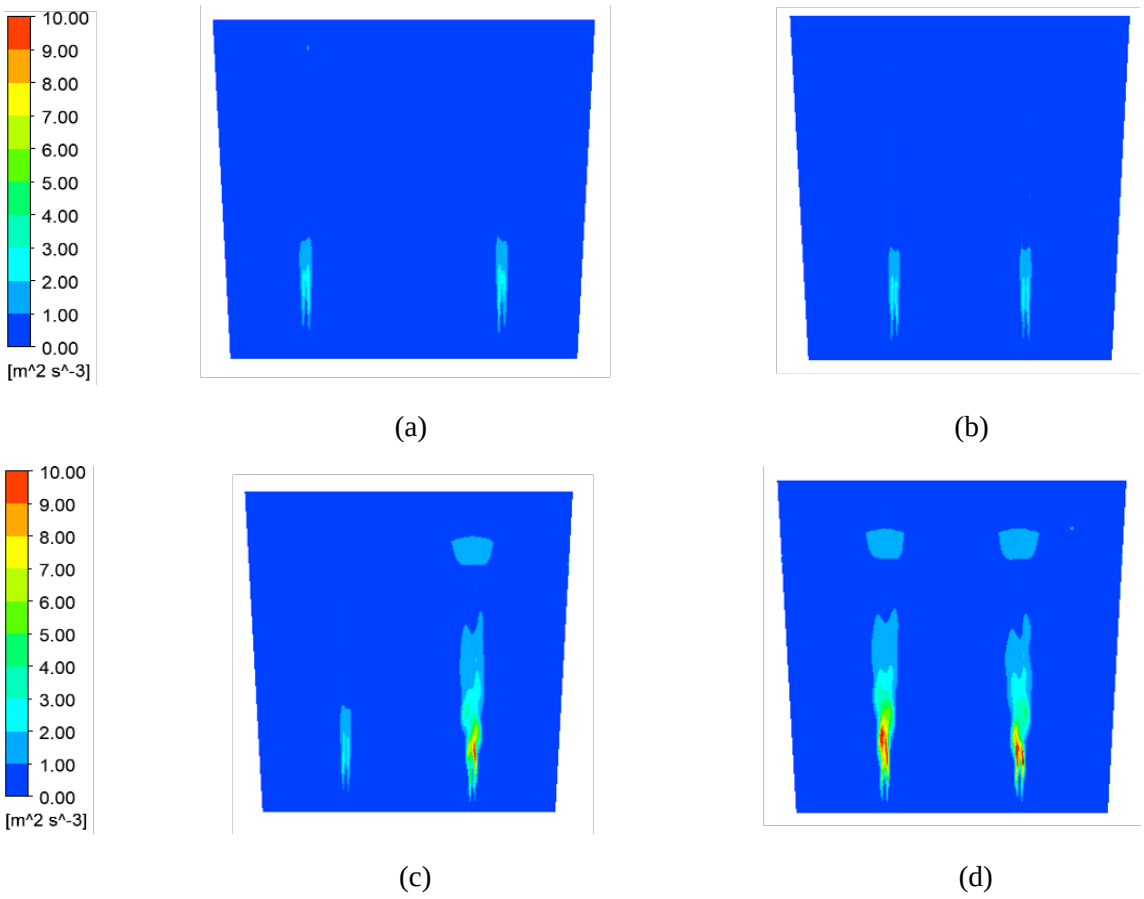

Figure 18. Turbulence dissipation rate for different cases (Plane ID refer to Figure 10): (a) 180° 5/5 SCFM, plane 1; (b) 90° 5/5 SCFM, plane 2; (c) 90° 5/20 SCFM, plane 2; (d) 90° 20/20 SCFM, plane 2

Table 8. Volume average turbulence dissipation rate for four cases

Case	Case 1 (180° 5/5 SCFM)	Case 2 (90° 5/5 SCFM)	Case 3 (90° 5/20 SCFM)	Case 4 (90° 20/20 SCFM)
ε (m^2/s^3 Volume Average)	0.0075	0.0072	0.0213	0.0353

3.4.3 Inclusion Aggregation and Removal in Full-Scale Ladle

As mentioned previously, inclusion removal includes six different mechanisms. They are inclusion removal due to wall adhesion, slag absorption, turbulence shear collision, turbulence random collision, turbulence buoyancy collision and bubble wake capture. The last four mechanisms are considered when inclusions collide with bubbles. But in this process, the bubble is only the carrier

that transports the inclusion to the slag or walls. After bubble breakup, inclusion will be eventually removed by slag or wall. But in order to find out how much inclusion will be carried by bubble, the bubble removal mechanisms must be defined. In this study, inclusion removal mechanism contribution will be examined using different ladle designs and flow rates.

3.4.3.1 Baseline case (180°, 5/5 SCFM) inclusion aggregation and removal analyze

Table 9 shows volume fraction distribution for different size of inclusions at 0 second, 100 seconds, 200 seconds and 300 seconds. Initially, there is mainly small size inclusion in the ladle. As time goes by, bigger size inclusion is formed due to inclusion aggregation.

Table 9. Inclusion size volume fraction change with time, 180° ladle, 5/5 SCFM

Size (μm)	0s	100s	200s	300s
5.0	55.0%	40.2%	35.0%	34.1%
6.3	30.0%	29.0%	27.5%	27.4%
7.9	11.0%	16.6%	18.5%	19.4%
10.0	4.0%	7.5%	9.0%	9.5%
10.3	0.0%	2.1%	3.1%	3.5%
10.6		1.1%	1.7%	1.7%
20.0		0.9%	1.5%	1.3%
25.2		0.7%	1.3%	1.1%
30.7		0.5%	0.9%	0.9%
40.0		0.7%	0.7%	0.5%
50.0		0.7%	0.8%	0.7%

Figure 19 shows 180° ladle inclusion phase volume fraction change with time. It can be seen that as time goes by, inclusion volume fraction decreases because of the inclusion removal mechanisms. According to Wang et al. [19], bubble detachment can be assumed to be zero and there is no slag eye formed at the top, so all the inclusion carried by the bubbles will be removed eventually. Therefore, when an inclusion is captured by a bubble, it is considered to be immediately removed. This is the reason for the two “clean steel” regions in the gas plume. During the refining process, inclusions in the steel will flow to plume region and interact with bubble, and “clean steel” will move to slag and wrap towards the wall, making recirculation regions.

Over time, the low inclusion volume fraction region will continue to expand from top to bottom of the ladle until nearly all inclusions have been removed. The volume fraction distribution can be

used to identify the ladle mixing dead zones, mainly located at bottom corners of ladle and center of ladle between two plume regions.

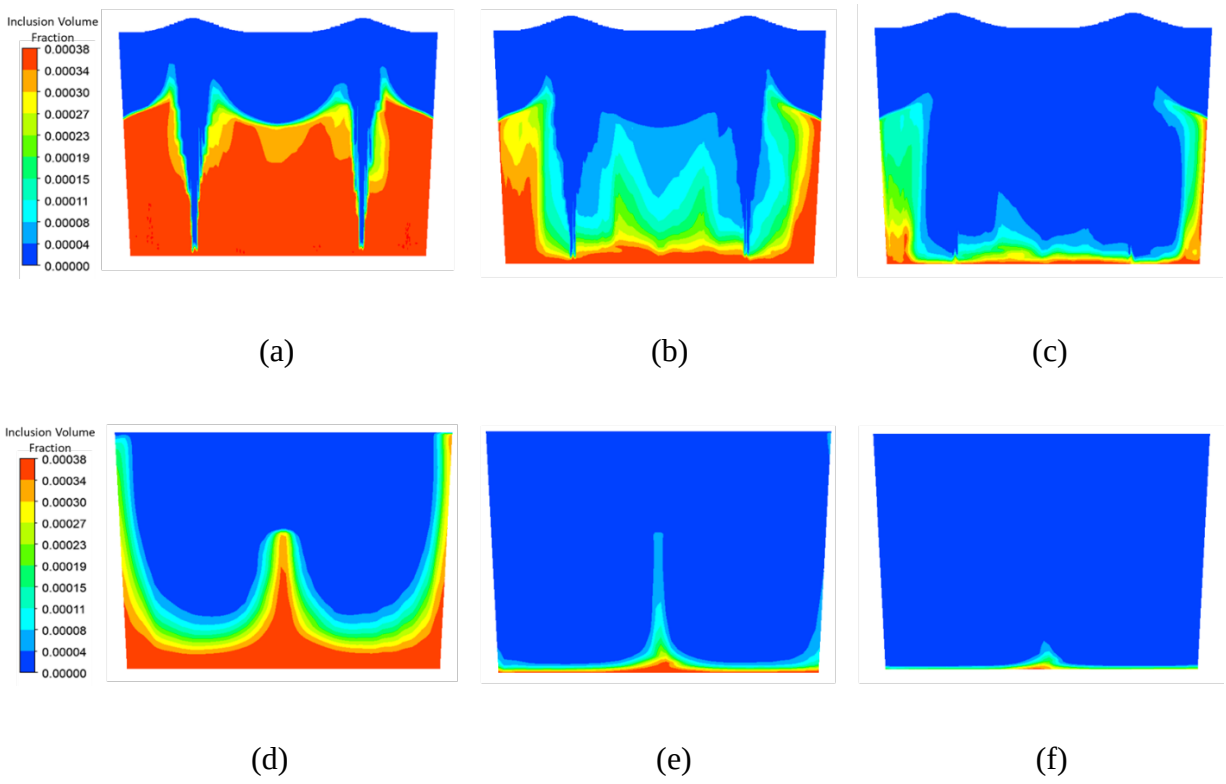

Figure 19. Contour of inclusion volume fraction change with time in 180° ladle, 5/5 SCFM: (a) 100 seconds, plane 1; (b) 200 seconds, plane 1; (c) 300 seconds, plane 1; (d) 100 seconds, plane 3; (e) 200 seconds, plane 3; (f) 300 seconds, plane 3

Figure 20 shows inclusion number density distribution versus time. It can be found that from 0 seconds, inclusion aggregation and removal shows a high efficiency. That is because of the use of fully developed flow field as the initial condition for the case. When inclusions are patched into the flow, the aggregation and removal mechanisms quickly act on the inclusions. In general, number density of different inclusion sizes shows a decreasing trend and the overall inclusion number density keeps decreasing as time goes by.

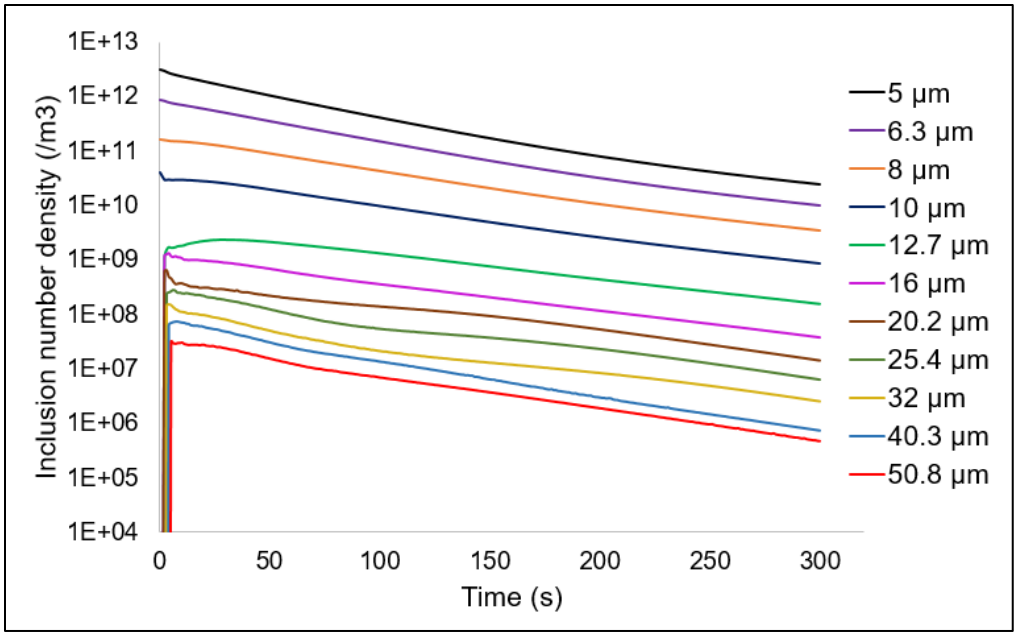

Figure 20. Inclusion number density change with time in 180° ladle, 5/5 SCFM

3.4.3.2 Inclusion aggregation and removal parametric study

Inclusion aggregation and removal in two-plug ladle with separation angles of 180° and 90° will be compared. For the 90° ladle, three different flow rate combination will be presented. It should be noted that for the 5/20 SCFM and 20/20 SCFM in the 90° ladle, the flow created an open slag eye. But since the inclusion re-release mechanism is not considered yet in this study, so numerically the overall inclusion removal rate for these two cases will be over predicted. In order to roughly study the effect of slag eye size on inclusion removal, mass percentage of bubble rupture at the slag eye interface has been recorded. Inclusion removal due to bubble capture is also recorded. As mentioned before, if a bubble ruptures at slag eye area, the transported inclusions will be released back into the steel, so the inclusion contained in the bubble that ruptures in the slag eye area should not be counted as having been removed. In this case, the final amount of inclusions removed should be deducted from the amount of inclusion in these bubbles.

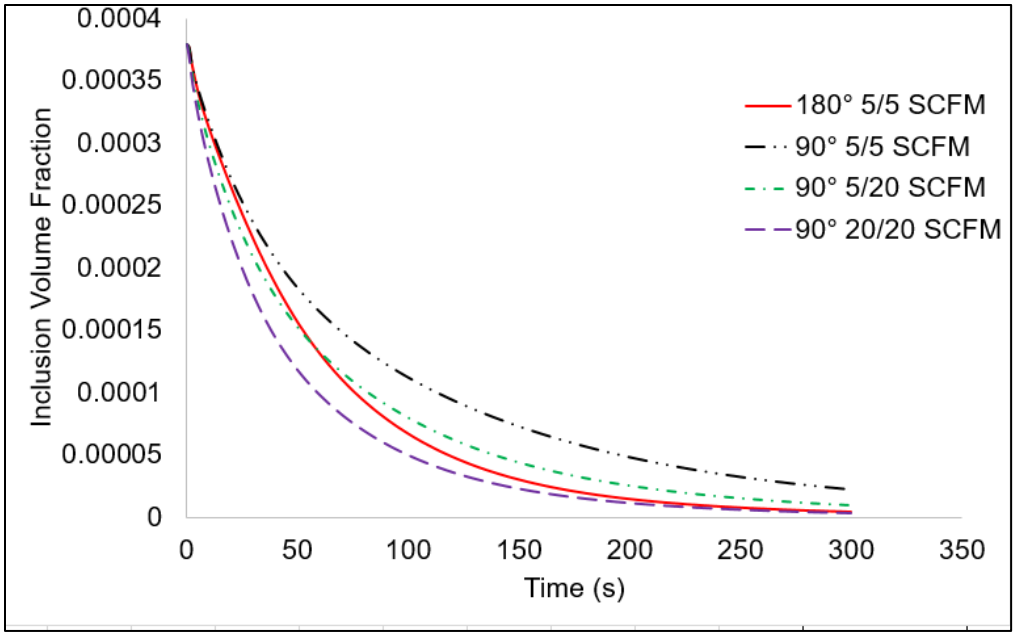

Figure 21. Inclusion phase volume fraction change with time in four cases

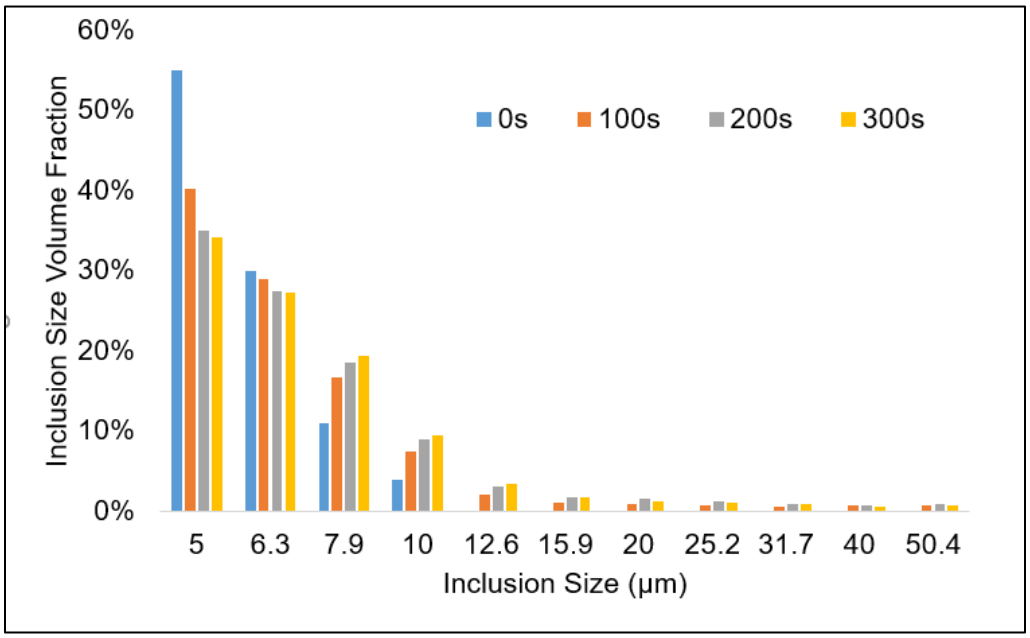

(a)

Figure 22. Inclusion size volume fraction distribution with time in four cases: (a) 180° 5/5 SCFM; (b) 90° 5/5 SCFM; (c) 90° 5/20 SCFM; (d) 90° 20/20 SCFM

Figure 22. Continued

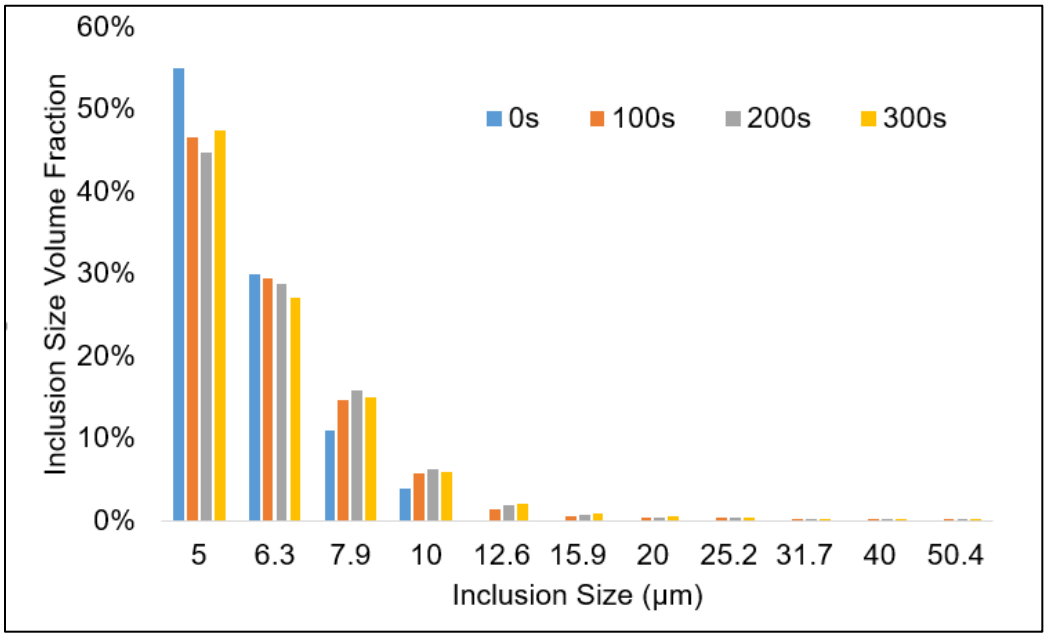

(b)

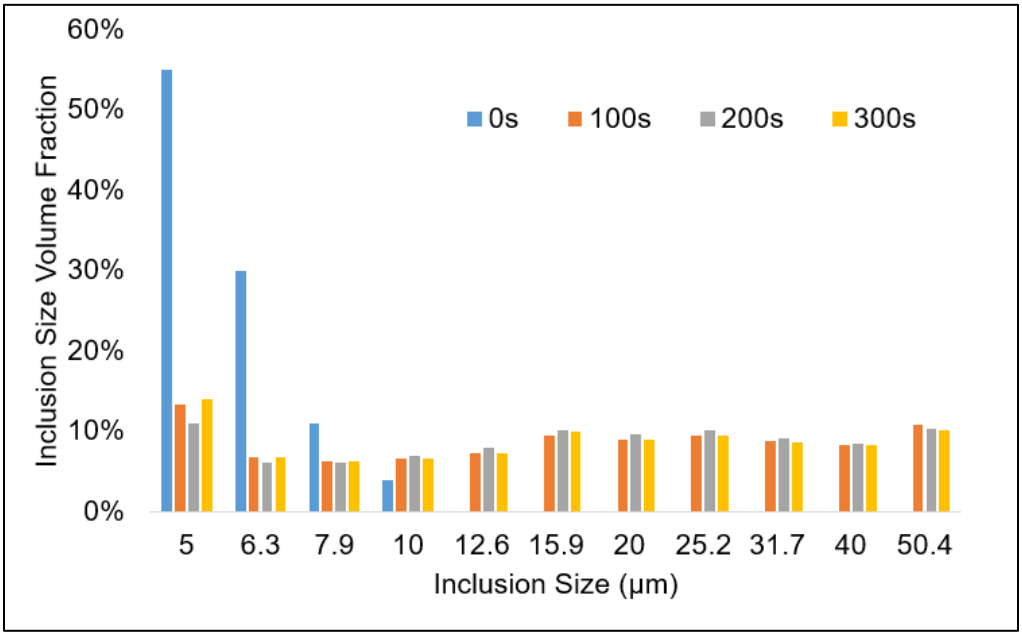

(c)

Figure 22. Continued

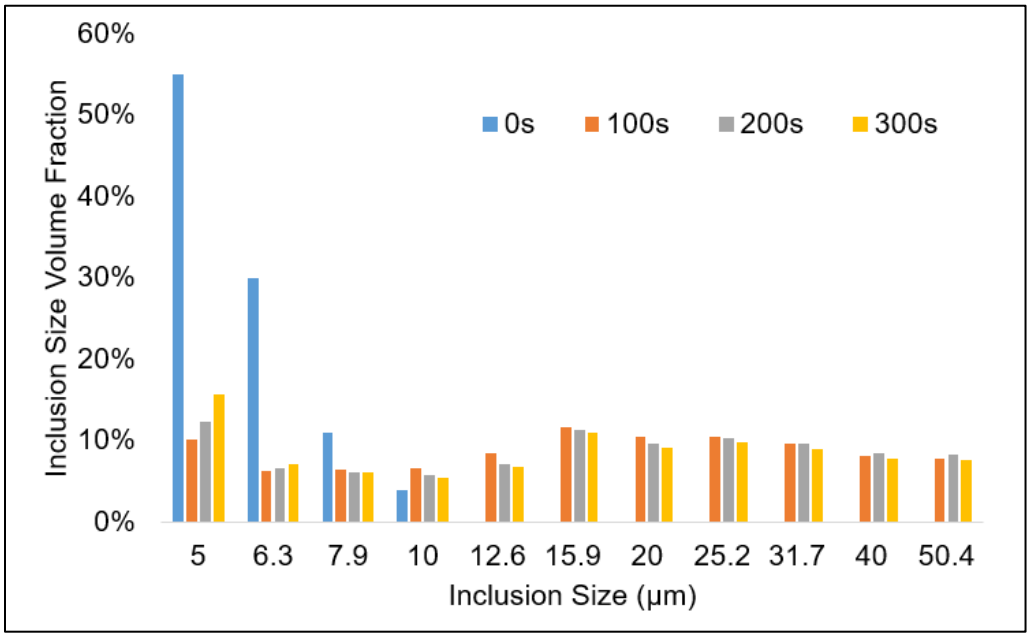

(d)

Figure 21 shows the overall inclusion phase volume fraction and size volume fraction change over time for four different cases. When inclusion release back from slag eye is not considered, fixing the plug position, as the argon flow rate increases, the inclusion removal rate will increase. When the argon flow rate is fixed, 180° ladle have better removal efficiency than 90° ladle. Figure 22 shows inclusion size volume fraction distribution in four cases. By (a) to (d) in Figure 22, when flow rate increase, the volume fraction of large size inclusion significant rise. That is because inclusion aggregation rate increases with flow rate increasing.

As mentioned before, turbulence dissipation rate is positively related to inclusion aggregation and removal. So as shown in Figure 18 and Table 8, under same plug position, turbulence dissipation rate increases as flow rate increases. With flow rate fixed, larger plug separation angle results in a turbulence dissipation rate increase.

The volume of the bubble plume is another important factor for inclusion removal.

Figure 23 shows the volume of bubble plume in different ladles. Table 10 lists the detailed volume of bubble plume in different ladles. From the table, the total bubble plume volume for the 180° ladle is slightly bigger than 90°; for the 90° ladle, as the flow rate increases, the volume will also increase. In the 90° ladle cases, there is no slag eye formed in the 5/5 SCFM case, but if the flow

rate increases from 5 SCFM to 20 SCFM, slag eye will be formed. When we compare case 2 (5/5 SCFM) and case 4 (20/20 SCFM), case 2 has no slag eye formed while case 4 has two slag eye appear at top. Even the volume of bubble plume of case 4 (3.03 m^3) is greater than case 2 (2.03 m^3), the inclusion removal rate for case 4 (89.66%) is still smaller than case 2 (94.08%), which means slag eye have more significant influence on inclusion removal compared to the volume of bubble plume. If we compare case 3 and case 4, case 3 has only one slag eye appear at the top, the total slag eye area is smaller than case 4, but the inclusion removal rate of case 3 is smaller than case 4. That is because in case 4, the volume of bubble plume is greater than case 3. With a larger bubble plume, inclusions have more of a chance to interact and be attached to bubbles. In this situation, more inclusions will be carried by bubbles moving to the slag-steel interface.

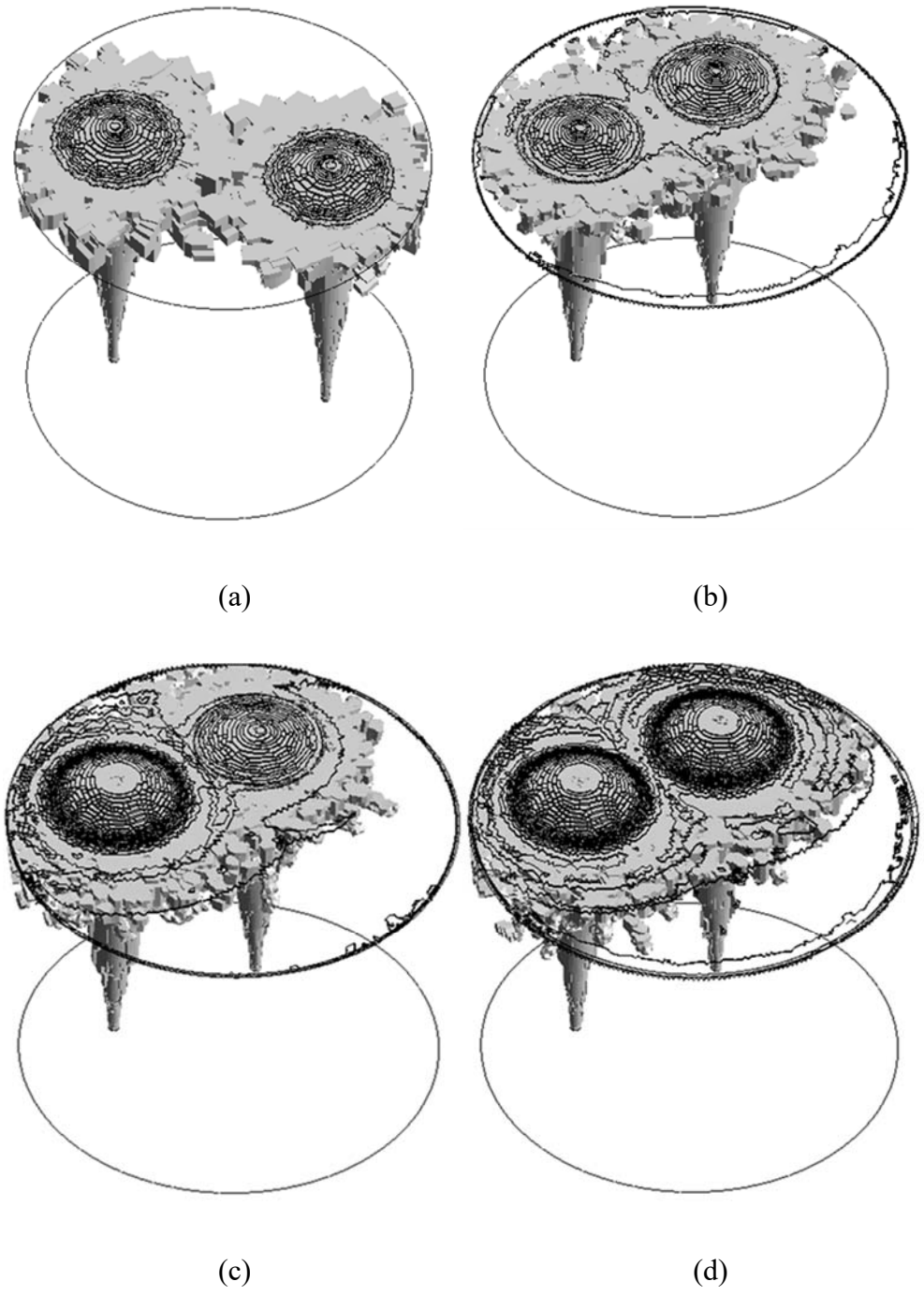

Figure 23. Volume of bubble mass fraction >= 1×10^{-8} in different cases: (a) 180° 5/5 SCFM; (b) 90° 5/5 SCFM; (c) 90° 5/20 SCFM; (d) 90° 20/20 SCFM

Table 10. Volume of bubble mass fraction >= 1×10^{-8} in different cases

	Case 1 (180° 5/5 SCFM)	Case 2 (90° 5/5 SCFM)	Case 3 (90° 5/20 SCFM)	Case 4 (90° 20/20 SCFM)
volume(m^3)	2.05	2.03	2.56	3.03

Table 11 shows inclusion removal rate, mass percentage of bubble rupture at slag eye and inclusion removal rate under consideration of bubble rupture in slag eye for all four cases.

Table 12 shows the percentage contribution of inclusion removal mechanisms. When bubble rupture at slag eye area is considered, the overall removal rate will decrease. Slag eye has a negative influence on inclusion removal. So gentle stirring is needed for inclusion removal process.

Table 11. Weight percentage of bubble rupture

	Case 1 (180° 5/5 SCFM)	Case 2 (90° 5/5 SCFM)	Case 3 (90° 5/20 SCFM)	Case 4 (90° 20/20 SCFM)
Weight percentage	0%	0%	11.12%	9.55%

Table 12. Removal mechanisms and overall removal rate for different cases

	Case 1 (180° 5/5 SCFM)	Case 2 (90° 5/5 SCFM)	Case 3 (90° 5/20 SCFM)	Case 4 (90° 20/20 SCFM)
Slag	3.55%	8.19%	4.23%	2.45%
Wall	0.00001%	0.00001%	0.00001%	0.00001%
Bubble	96.45%	91.81%	95.77%	97.55%
Overall	98.75%	94.08%	97.58%	99.07%
Overall (considered bubble rupture at slag eye)	98.75%	94.08%	86.78%	89.66%

4 CONCLUSION

The comprehensive study of inclusion aggregation and removal in different bottom gas-stirred ladles has been conducted. The unsteady, three dimensional, isothermal, multiphase computational fluid dynamics (CFD) model was developed. A ladle with two bottom plugs was used in the study. Effects of plug separation angles (180° and 90°) and argon flow rate combinations (5/5 SCFM, 5/20 SCFM and 20/20 SCFM) were investigated. The whole study can be divided into two part: first, the flow field, slag eye size and wall shear stress have been studied; second, inclusion aggregation and removal in different ladles have been investigated.

In the first part, argon bubble breakup and coalescence has been considered. Flow field in four different cases are studied. The slag eye appears at 90°, 5/20 SCFM case and 90°, 20/20 SCFM cases. The mean diameter of slag eye for these two cases is 0.64m and 0.62m respectively. As for wall shear stress, flow rate and plug separation angle increase can result in maximum wall shear stress increase. The maximum wall shear stress is 8.07 Pa on 90°, 5/20 SCFM case and 90°, 20/20 SCFM case.

In the second part, a parametric study of ladle design and flow rate on inclusion aggregation and removal has been conducted. Without considering slag eye release back mechanism, when the gas flow rate is fixed, the plug separation angle increases, the inclusion removal rate will increase; when the plug separation angle is fixed, the gas flow rate increases, and the inclusion removal rate will increase as well. When bubble rupture at slag eye assumption is considered, the overall inclusion removal rate will decrease 10.8% and 9.41% for the 90°, 5/20 SCFM case and the 90°, 20/20 SCFM case respectively.

REFERENCES

[1] Lou, Wentao, and Miaoyong Zhu. "Numerical simulations of inclusion behavior in gas-stirred ladles." Metallurgical and Materials Transactions B 44.3 (2013): 762-782

[2] J. Szekely, S. Asai, Trans. Iron Steel Inst. Jpn., (1975), 15, 270.

[3] T. DebRoy, A. K. Majumdar, D. B. Spalding, Appl. Math. Model., (1978) 2, 146.

[4] S. T. Johansen, D. G. C. Robertson, K. Woje, T. Engh, *Metall. Mater. Trans. B*, (1988), *19*, 745.

[5] Peranandhanthan, M., and Dipak Mazumdar. "Modeling of slag eye area in argon stirred ladles." ISIJ international 50.11 (2010): 1622-1631.

[6] Mazumdar, Dipak, and Roderick IL Guthrie. "Modeling energy dissipation in slag-covered steel baths in steelmaking ladles." Metallurgical and Materials Transactions B 41.5 (2010): 976-989.

[7] Guo, D., & Irons, G. A. (2000). Modeling of gas-liquid reactions in ladle metallurgy: Part II. Numerical simulation. Metallurgical and Materials Transactions B, 31(6), 1457-1464.

[8] L. Zhang, *Modell. Simul. Mater. Sci. Eng*., (2000), *8,* 463.

[9] Lou, Wentao, and Miaoyong Zhu. "Numerical simulation of gas and liquid two-phase flow in gas-stirred systems based on Euler–Euler approach." Metallurgical and Materials Transactions B 44.5 (2013): 1251-1263.

[10] Cao, Qing, and L. Nastac. "Mathematical Investigation of Fluid Flow, Mass Transfer, and Slag-steel Interfacial Behavior in Gas-stirred Ladles." Metallurgical & Materials Transactions B (2018):1-17.

[11] Zhang, Lifeng. "Nucleation, growth, transport, and entrapment of inclusions during steel casting." Jom 65.9 (2013): 1138-1144.

[12] Zhang, Lifeng, Wolfgang Pluschkell, and Brian G. Thomas. "Nucleation and growth of alumina inclusions during steel deoxidation." Steelmaking Conference Proceedings. Vol. 85. 2002

[13] Shirabe.K, Szekely. J. A Mathematical Model Fluid Flow Inclusion Coalescence RH Vacuum Degassing System. ISIJ , Int.,1983,23(3):465

[14] Johansen S. T,. Boysan F. and Engh T.A,. Numerical calculations of removal of inclusions and dissolution of refractory in a bubble stirred ladel., Procceedings Fourth Japan-Nordic

[15] Hallberg M., En Matematisk modell for desoxidation av en omrord stalsmalta,. Tech. lic. Royal Institute of Technology (1996), ISSN 0281-8604, ISBN 91-7170-949-2

[16] Wakoh M., Fuchigami K., Endoh K., Imamura N., Kiyose A. and Sawada I., Analysis of inclusion behavior in a ladle refining process by using newly developed coagulation model., Scanmet I, Lulea, Sweden,June, 1999, pp.267-274

[17] Miki Y. and Thomas B.G., Modeling of inclusion removal in a tundish. Metallurgical and Materials Transactions B, vol 30B(1999) pp.639-654

[18] Söder, Mats, P. Jönsson, and L. Jonsson. "Inclusion Growth and Removal in Gas-Stirred Ladles." *Steel Research International* 75.2(2004):128-138.

[19] Wang, Li Tao, et al. "Mathematical Model for Growth and Removal of Inclusions in Molten Steel under Gas-stirring Conditions." *Steel Research International* 77.1(2006):25-31.

[20] Harmathy, Tibor Z. "Velocity of large drops and bubbles in media of infinite or restricted extent." AIChE Journal 6.2 (1960): 281-288.

[21] Fluent, A. N. S. Y. S. "Theory guide." Ansys Inc.: Canonsburg, PA, USA (2015).

[22] H. Laux, S. T. Johansen, “A CFD analysis of the air entrainment rate due to a plunging steel jet combining mathematical models for dispersed and separated multiphase flows,” *Minerals, Metals and Materials Society Symposium*, San Diego, CA, 1999.

[23] Q. Pan, "Modelling of Turbulent Flows with Strong Dispersed Phase-Continuous Fluid Interactions," *Doctoral Thesis*, NTNU, Trondheim, (2014).

[24] Johansen, S. T., and F. Boysan. "Fluid dynamics in bubble stirred ladles: Part II. Mathematical modeling." Metallurgical Transactions B 19.5 (1988): 755-764.

[25] Lou, Wentao, and Miaoyong Zhu. "Numerical simulation of desulfurization behavior in gas-stirred systems based on computation fluid dynamics–simultaneous reaction model (CFD–SRM) coupled model." Metallurgical and Materials Transactions B 45.5 (2014): 1706-1722.

[26] Krishnapisharody, Krishnakumar, and Gordon A. Irons. "An extended model for slag eye size in ladle metallurgy." ISIJ international 48.12 (2008): 1807-1809.

PUBLICATION

Liu, Wenjie, et al. "Argon Bubble Coalescence and Breakup in a Steel Ladle with Bottom Plugs." *steel research international*90.4 (2019): 1800396.